



# Jefferson Lab PAC21 Proposal Cover Sheet

This document must  
be received by close  
of business Monday,

Dec. 3, 2001 at:

Jefferson Lab  
User/International Liaison  
Mail Stop 12B  
12000 Jefferson Ave.  
Newport News, VA  
23606

Experimental Hall: \_\_\_\_\_ C \_\_\_\_\_

Days Requested for Approval: \_\_\_\_\_ 45 \_\_\_\_\_

**Proposal Title:**

The Neutron Electric Form Factor at  $Q^2 = 2.40 \text{ (GeV/c)}^2$

### Proposal Physics Goals

Indicate any experiments that have physics goals similar to those in your proposal.

### Approved, Conditionally Approved, and/or Deferred Experiment(s) or proposals:

E01-001 for GEp  
E01-109 for GEp/GMp

### Contact Person

**Name:** Richard Madey

**Institution:** Kent State University & Jefferson Lab

**Address:** Kent, OH 44242 &

**Address:** Newport News, VA 23606

**City, State, ZIP/Country:** USA

**Phone:** (757) 269-7323

**Fax:** (757) 269-6273

**E-Mail:** madey@jlab.org

**Jefferson Lab Use Only**

Receipt Date: \_\_\_\_\_

By: \_\_\_\_\_

# LAB RESOURCES LIST

JLab Proposal No.: \_\_\_\_\_  
*(For JLab ULO use only.)*

Date November 28, 2001

List below significant resources — both equipment and human — that you are requesting from Jefferson Lab in support of mounting and executing the proposed experiment. Do not include items that will be routinely supplied to all running experiments such as the base equipment for the hall and technical support for routine operation, installation, and maintenance.

## **Major Installations** *(either your equip. or new equip. requested from JLab)*

- Neutron Polarimeter & Enclosure
- Dipole Magnet [Charybdis]
- Steel Shadow Shield
- Lead Curtain

### *New Support Structures:*

- Shield House & Collimator for Polarimeter
- Support Structure for Polarimeter
- Support Structure for Shadow Shield

## **Data Acquisition/Reduction**

### *Computing Resources:*

### *New Software:*

## **Major Equipment**

Magnets: -HMS  
-Charybdis

Power Supplies: -HMS  
-SOS [for Charybdis]

Targets: -LD2  
-LH2  
-Dummy

Detectors: -Additional Detectors for Polarimeter

Electronics:

Computer Hardware:

Other: -Moeller Polarimeter

**Other:**

# BEAM REQUIREMENTS LIST

JLab Proposal No.: \_\_\_\_\_ Date: November 28, 2001

Hall:   c   Anticipated Run Date: \_\_\_\_\_ PAC Approved Days: \_\_\_\_\_

Spokesperson: Richard Madey

Hall Liaison: \_\_\_\_\_

Phone: (757) 269-7323

E-mail: madey@jlab.org

List all combinations of anticipated targets and beam conditions required to execute the experiment. (This list will form the primary basis for the Radiation Safety Assessment Document (RSAD) calculations that must be performed for each experiment.)

Condition No.	Beam Energy (MeV)	Mean Beam Current ( $\mu$ A)	Polarization and Other Special Requirements (e.g., time structure)	Target Material (use multiple rows for complex targets — e.g., w/windows)	Material Thickness (mg/cm <sup>2</sup> )	Est. Beam-On Time for Cond. No. (hours)
C1	5000	10	> 70% Polarization	15-cm LD2	2430	24
C2	5000	1	> 70% Polarization	Fe	8	24
C3	5000	10	> 70% Polarization	15-cm LD2	2430	62
1	5000	60	> 70% Polarization	15-cm LD2	2430	658
2	5000	90	> 70% Polarization	15-cm LH2	1065	96
3	5000	40	> 70% Polarization	Al	583	72
4	5000	1	> 70% Polarization	Fe	8	72

The beam energies,  $E_{\text{Beam}}$ , available are:  $E_{\text{Beam}} = N \times E_{\text{Linac}}$  where  $N = 1, 2, 3, 4, \text{ or } 5$ .  $E_{\text{Linac}} = 800$  MeV, i.e., available  $E_{\text{Beam}}$  are 800, 1600, 2400, 3200, and 4000 MeV. Other energies should be arranged with the Hall Leader before listing.

# HAZARD IDENTIFICATION CHECKLIST

JLab Proposal No.: \_\_\_\_\_

Date: November 28, 2001

(For CEBAF User Liaison Office use only.)

Check all items for which there is an anticipated need.

<p><b>Cryogenics</b></p> <p><input type="checkbox"/> beamline magnets</p> <p><input type="checkbox"/> analysis magnets</p> <p><input checked="" type="checkbox"/> target</p> <p>type: <u>LD2, LH2</u></p> <p>flow rate: _____</p> <p>capacity: _____</p>	<p><b>Electrical Equipment</b></p> <p><input type="checkbox"/> cryo/electrical devices</p> <p><input type="checkbox"/> capacitor banks</p> <p><input type="checkbox"/> high voltage</p> <p><input type="checkbox"/> exposed equipment</p>	<p><b>Radioactive/Hazardous Materials</b></p> <p>List any radioactive or hazardous/toxic materials planned for use:</p>
<p><b>Pressure Vessels</b></p> <p>_____ inside diameter</p> <p>_____ operating pressure</p> <p>_____ window material</p> <p>_____ window thickness</p>	<p><b>Flammable Gas or Liquids</b></p> <p>type: _____</p> <p>flow rate: _____</p> <p>capacity: _____</p> <p><b>Drift Chambers</b></p> <p>type: _____</p> <p>flow rate: _____</p> <p>capacity: _____</p>	<p><b>Other Target Materials</b></p> <p><input type="checkbox"/> Beryllium (Be)</p> <p><input type="checkbox"/> Lithium (Li)</p> <p><input type="checkbox"/> Mercury (Hg)</p> <p><input type="checkbox"/> Lead (Pb)</p> <p><input type="checkbox"/> Tungsten (W)</p> <p><input type="checkbox"/> Uranium (U)</p> <p><input checked="" type="checkbox"/> Other (list below)</p> <p style="margin-left: 20px;">Aluminum Dummy Fe (for Moeller Polarimeter)</p>
<p><b>Vacuum Vessels</b></p> <p>_____ inside diameter</p> <p>_____ operating pressure</p> <p>_____ window material</p> <p>_____ window thickness</p>	<p><b>Radioactive Sources</b></p> <p><input type="checkbox"/> permanent installation</p> <p><input checked="" type="checkbox"/> temporary use</p> <p>type: <u>228 Thorium</u></p> <p>strength: <u>~10 uC</u></p>	<p><b>Large Mech. Structure/System</b></p> <p><input type="checkbox"/> lifting devices</p> <p><input type="checkbox"/> motion controllers</p> <p><input checked="" type="checkbox"/> scaffolding or</p> <p><input checked="" type="checkbox"/> elevated platforms</p>
<p><b>Lasers</b></p> <p>type: _____</p> <p>wattage: _____</p> <p>class: _____</p> <p>Installation:</p> <p><input type="checkbox"/> permanent</p> <p><input type="checkbox"/> temporary</p> <p>Use:</p> <p><input type="checkbox"/> calibration</p> <p><input type="checkbox"/> alignment</p>	<p><b>Hazardous Materials</b></p> <p><input type="checkbox"/> cyanide plating materials</p> <p><input type="checkbox"/> scintillation oil (from)</p> <p><input type="checkbox"/> PCBs</p> <p><input type="checkbox"/> methane</p> <p><input type="checkbox"/> TMAE</p> <p><input type="checkbox"/> TEA</p> <p><input type="checkbox"/> photographic developers</p> <p><input type="checkbox"/> other (list below)</p>	<p><b>General:</b></p> <p>Experiment Class:</p> <p><input type="checkbox"/> Base Equipment</p> <p><input type="checkbox"/> Temp. Mod. to Base Equip.</p> <p><input type="checkbox"/> Permanent Mod. to Base Equipment</p> <p><input checked="" type="checkbox"/> Major New Apparatus</p> <p>Other: <u>Polarimeter</u></p>

# Computing Requirements List

**Proposal Title:** The Neutron Electric Form Factor at  $Q^2 = 2.40 \text{ (GeV/c)}^2$

**Spokesperson:** Richard Madey **Experimental Hall:** C

## Raw Data Expected

**Total:** 200 GB **Per Year (long duration experiments only):** \_\_\_\_\_

**Simulation Compute Power (SPECint95 hours) Required:** 1000 hours CPU on ifarm1

**On-Line Disk Storage Required:** 300 GB work space

**Imported Data Amount from Outside Institutions:** \_\_\_\_\_

**Exported Data Amount to Outside Institutions:** \_\_\_\_\_

**Expected Mechanism for Imported/Exported Data:** \_\_\_\_\_

## Special Requirements

For example, special configuration of data acquisition systems) that may require resources and/or coordination with JLab's Computer Center. Please indicate, if possible, what fraction of these resources will be provided by collaborating institutions and how much is expected to be provided by JLab.

Submit

## The Neutron Electric Form Factor at $Q^2 = 2.40 \text{ (GeV/c)}^2$

*Spokesman: R. Madey, Kent State University & Jefferson Lab*

*Co-Spokesman: S. Kowalski, Massachusetts Institute of Technology*

### Abstract

We propose to extend measurements of the electric form factor of the neutron,  $G_E^n$ , to a squared four-momentum transfer of  $2.40 \text{ (GeV/c)}^2$ . The JLab E93-038 collaboration conducted  $d(\vec{e}, e'\vec{n})p$  measurements on a liquid deuterium target from September 8, 2000 to April 26, 2001 at  $Q^2$  values of 0.45, 1.15, and  $1.47 \text{ (GeV/c)}^2$ . *Polarization measurements above  $Q^2 \approx 1 \text{ (GeV/c)}^2$  require the beam energies available at CEBAF. In the technique demonstrated in E93-038 with a high-luminosity, high-efficiency neutron polarimeter and the dipole neutron-spin-precession magnet [Charybdis], we measured the ratio of two scattering asymmetries associated with positive and negative precessions of the neutron polarization vector.* In this ratio technique, systematic uncertainties are small because the analyzing power of the polarimeter cancels in the ratio, and the beam polarization cancels also because, as demonstrated in E93-038, the beam polarization does not change much in sequential measurements of the two scattering asymmetries.

The primary motivation for this measurement is the unique ability to measure a fundamental quantity of the neutron — one of the basic building blocks of matter. The proposed measurement of  $G_E^n$  will be available to challenge rigorous Lattice QCD calculations. This measurement of  $G_E^n$  is needed to understand electron scattering experiments that probe electric structure functions at high  $Q^2$ ; it is important for the analysis of few-body data near  $Q^2 = 2.4 \text{ (GeV/c)}^2$ , which is right in the middle of the  $Q^2$  range for all few body measurements at Jefferson Lab. Extension of E93-038 to a higher  $Q^2$  will improve the precision of the interior charge density.

## List of Participants

R. Madey (Spokesman), B.D. Anderson (Institutional Representative), A.R. Baldwin,  
D.M. Manley, A.Yu. Semenov, W. Tireman, J.W. Watson, W.-M. Zhang, C. Yan  
Kent State University

R. Carlini (*Institutional Representative*), R. Ent, H. Fenker, K. Garrow, M. Jones, A. Lung,  
D. Mack, G. Smith, W. Vulcan, S. Wood, C. Yan  
Thomas Jefferson National Accelerator Facility

S. Kowalski (Co-Spokesman and Institutional Representative), M. Farkhondeh, B. Plaster,  
S. Taylor  
Massachusetts Institute of Technology

S. Churchwell, C. Howell (*Institutional Representative*), S. Tajima  
Duke University

H. Breuer, J.J. Kelly (*Institutional Representative*), N. Savvinov  
University of Maryland

E. Crouse, J.M. Finn (*Institutional Representative*), C. Perdrisat  
The College of William and Mary

O.K. Baker (*Institutional Representative*), E. Christy, L. Cole, A. Gasparian, P. Gueye, B. Hu,  
C. Keppel, L. Tang, L. Yuan  
Hampton University

A. Ahmidouch (*Institutional Representative*), S. Danagoulian  
North Carolina A&T State University

G. MacLachlan, A. Opper (*Institutional Representative*)  
Ohio University

A. Aghalaryan, R. Asaturyan, H.G. Mkrtchyan (*Institutional Representative*), S. Stepanyan,  
V. Tadevosyan  
Yerevan Physics Institute

## List of Participants (continued)

S. Wells (*Institutional Representative*), N. Simicevic  
Louisiana Tech

P. Markowitz (*Institutional Representative*), B. Raue, J. Reinhold  
Florida International University

D. Day (*Institutional Representative*), F. Wesselmann, H. Zhu  
University of Virginia

P. Ulmer  
Old Dominion University

M. Khandaker (*Institutional Representative*), V. Punjabi  
Norfolk State University

M. Elaasar  
Southern University at New Orleans

R.E. Segel  
Northwestern University

R. Wilson  
Harvard University

W.-Y. Kim (*Institutional Representative*), W. Seo  
Kyungpook National University

T. Reichelt  
University of Bonn

L. Gan  
University of North Carolina at Wilmington

H. Arenhovel  
University of Mainz

# Contents

<b>Abstract</b>	<b>i</b>
<b>List of Participants</b>	<b>ii</b>
<b>Contents</b>	<b>iv</b>
<b>List of Figures</b>	<b>v</b>
<b>List of Tables</b>	<b>vi</b>
<b>1 Scientific Motivation</b>	<b>1</b>
1.1 Extension of E93-038 to Measure $G_E^n$ at $Q^2 = 2.40 \text{ (GeV}/c)^2$	1
1.2 Improved Precision of Interior Charge Density	4
1.3 Better Knowledge of Neutron Structure	7
1.4 Better Understanding of Electron Scattering Data From Nuclei	10
<b>2 Theoretical Background</b>	<b>11</b>
<b>3 Description of the Experiment</b>	<b>13</b>
3.1 Experimental Arrangement	13
3.2 Kinematics	18
3.3 Count Rates	20
3.4 Projected Uncertainties	21
<b>4 Some Results from E93-038</b>	<b>26</b>
<b>5 Beam Time</b>	<b>32</b>
<b>6 Collaboration</b>	<b>32</b>
<b>References</b>	<b>34</b>
<b>Appendix A: Nucleon Charge and Magnetization Densities,     J.J. Kelly, Preprint</b>	<b>38</b>

# List of Figures

1	$G_E^n$ versus $Q^2$ . The line reflects the Galster parameterization of $G_E^n$ . . . . .	1
2	$G_E^n$ data extracted from the deuteron quadrupole form factor by Schiavilla and Sick (open circles) together with the results of JLab E93-038 preliminary measurements (filled squares). . . . .	2
3	$(G_E^n/G_D)^2$ as a function of $Q^2$ . The data plotted as filled circles are from SLAC-NE11 [Lung et al. (1993)]; the data plotted as open squares are from Hanson et al. (1973). The solid line is the Galster parameterization. The uncertainty projected in this proposal for $Q^2 = 2.40$ (GeV/c) <sup>2</sup> is for a value $(G_E^n/G_D)^2 = 0.0365$ , which is one-half of the Galster value. The filled squares are data from E93-038. . . . .	3
4	Comparison between fitted charge ( $\rho$ ) and magnetization ( $\mu$ ) densities for the proton. The error bands are tight and difficult to discern. . . . .	4
5	Charge ( $\rho$ ) and magnetization ( $\mu$ ) densities for the neutron. . . . .	5
6	Comparison of the FBE analysis of $G_E^n$ data with the two-parameter Galster parameterization. <i>The more general FBE parameterization permits more latitude in the extrapolation of the data to higher <math>Q^2</math>.</i> . . . . .	6
7	Some model predictions for $G_E^p$ (panel a) and $G_E^n$ (panel b). . . . .	8
8	Lattice QCD calculation result for $G_E^n$ . . . . .	9
9	Proton and neutron form factors as a function of $Q^2$ . The red solid line in the top panel is a parameterization from Eq. (4) for $G_E^p$ . . . . .	10
10	The ratio of isoscalar and isovector cross-sections [Eq. (6)] as a function of $Q^2$ . We assume the Galster parameterization for $G_E^n$ [Eq. (1)] and the parameterization from Eq. (4) for $G_E^p$ . The error bars for the presented points originate from the projected uncertainty $\Delta G_E^n = 0.0042$ and the uncertainty of the E93-027 measurement at $Q^2 = 2.47$ (GeV/c) <sup>2</sup> ( $\mu_p g_p = 0.726 \pm 0.027 \pm 0.062$ ). . . . .	12
11	Schematic diagram of the experimental arrangement. . . . .	14
12	Efficiency (top panel) and the analyzing power (bottom panel) of the E93-038 neutron polarimeter. Data obtained during the E93-038 run. . . . .	15
13	Singles rates for beam energy of 884 MeV and a CHARYBDIS current of -170 A. . . . .	16
14	Footprint in Hall C of the polarimeter shielding enclosure for a neutron angle of 40.9 degrees and a mean flight path of 9.0 m. The shielding enclosure is compatible with the setup for the G <sub>0</sub> experiment. . . . .	17
15	Statistical uncertainty, real event rate, and the polarization transfer, projected at $Q^2 = 2.4$ (GeV/c) <sup>2</sup> , as a function of beam energy. The statistical uncertainty increases for beam energies above $\approx 5$ GeV because the polarization transfer at a fixed $Q^2$ becomes smaller with increasing beam energy. . . . .	19
16	Statistical uncertainty, projected at $Q^2 = 2.4$ (GeV/c) <sup>2</sup> , as a function of precession angle. . . . .	20

17	Momentum distributions for electrons in the HMS associated with neutrons and protons scattered into the polarimeter. Panel (a) shows spectra obtained in E93-038 at $Q^2 = 1.47$ (GeV/c) <sup>2</sup> . Panel (b) demonstrates a result of a simulation at $Q^2 = 2.40$ (GeV/c) <sup>2</sup> . <i>The shift in the proton spectrum occurs because protons are deflected by the field of the Charybdis magnet. A cut on <math>\Delta p/p</math> (<math>= \pm 2\%</math>) reduces the false asymmetry or asymmetry dilution from the two step process <math>d(\vec{e}, e'\vec{p})n + Pb(\vec{p}, \vec{n})</math> in the lead curtain ahead of the polarimeter.</i> . . . . .	21
18	Real event rate, accidental coincidence rate, and the reals-to-accidentals ratio obtained from E93-038 and from a calculation at $Q^2 = 2.4$ (GeV/c) <sup>2</sup> . The target-front array flight path was 7 m for NPOL at 46 degrees, and 9 m for NPOL at 40.9 degrees. . . . .	23
19	Projected uncertainty $\Delta g_n/g_n$ as a function of the DAQ time. The beam current is 50 $\mu$ A, and the corrupted fraction (see text) is 25%. . . . .	24
20	Projected uncertainty $G_E^n$ as a function of the DAQ time for the Galster parameterization and $G_E^n = 0$ . The beam current is 50 $\mu$ A, and the corrupted fraction is 25%. . . . .	25
21	cTOF (top panel) and dTOF (bottom panel) spectra for run 39257 at $Q^2 = 1.47$ (GeV/c) <sup>2</sup> . . . . .	27
22	Four dTOF spectra (LU, LD, RU, and RD – see text) for run 39257 at $Q^2 = 1.47$ (GeV/c) <sup>2</sup> . . . . .	28
23	Asymmetries obtained from preliminary analysis of a data at $Q^2 = 1.47$ (GeV/c) <sup>2</sup> ( <b>not for quotation!</b> ). . . . .	29
24	Correlation between cTOF and dTOF for summary of four runs at $Q^2 = 1.14$ (GeV/c) <sup>2</sup> . . . . .	30
25	Event rate versus beam current at $Q^2 = 1.14$ (GeV/c) <sup>2</sup> . . . . .	31
26	Electron beam polarization in January 2001. . . . .	32
27	Calculated fraction of electron-neutron coincidence events corrupted from a background particle (charged or neutral) that appears during the coincidence time window of 70 ns as a function of the beam current. . . . .	33

## List of Tables

1	Kinematic conditions at a neutron scattering angle of 40.9° and a beam with a beam energy of 5.0 GeV. Also listed are the neutron energy resolution and the Charybdis field integral $B\Delta l$ required to precess the neutron polarization vector through $\pm 20$ degrees. . . . .	18
2	The neutron polarimeter and HMS acceptances, estimated neutron polarimeter parameters, and calculated real event rate at $Q^2 = 2.4$ (GeV/c) <sup>2</sup> . . . . .	22
3	Beam-time request for measuring $G_E^n$ at $Q^2 = 2.40$ (GeV/c) <sup>2</sup> for a 50 $\mu$ A, 70% polarized beam on a 15-cm LD <sub>2</sub> target. . . . .	34

# 1 Scientific Motivation

## 1.1 Extension of E93-038 to Measure $G_E^n$ at $Q^2 = 2.40$ (GeV/c)<sup>2</sup>

The electric form factor of the neutron,  $G_E^n$ , is a fundamental quantity needed for the understanding of both nucleon and nuclear structure. The dependence of  $G_E^n$  on  $Q^2$  reflects the distribution of charge in the neutron. The E93-038 collaboration carried out measurements of  $G_E^n$  from September 8, 2000 to April 26, 2001 at three values of  $Q^2$  [viz., 0.45, 1.15, and 1.47 (GeV/c)<sup>2</sup>]. Figure 1 is a plot of  $G_E^n$  versus  $Q^2$  of the world data from polarization measurements. Preliminary results of a first-pass analysis of the data from E93-038 indicate that  $G_E^n$  continues to follow the parameterization of Galster et al. (1971). The preliminary E93-038 points [**not for quotation**] are shown as filled squares. The E93-038 error bars are statistical and include a relative uncertainty in  $G_M^n$  of 5%. The Galster parameterization is plotted as a solid line in Fig. 1. Literature references to these data include Eden et al. (1994), Meyerhoff et al. (1994), Schmieden (1996), Klein and Schmieden (1997a), Klein (1997b), Ostrick et al. (1999), Herberg et al. (1999), Passchier et al. (1999), Rohe et al. (1999), and Zhu et al. (2001).

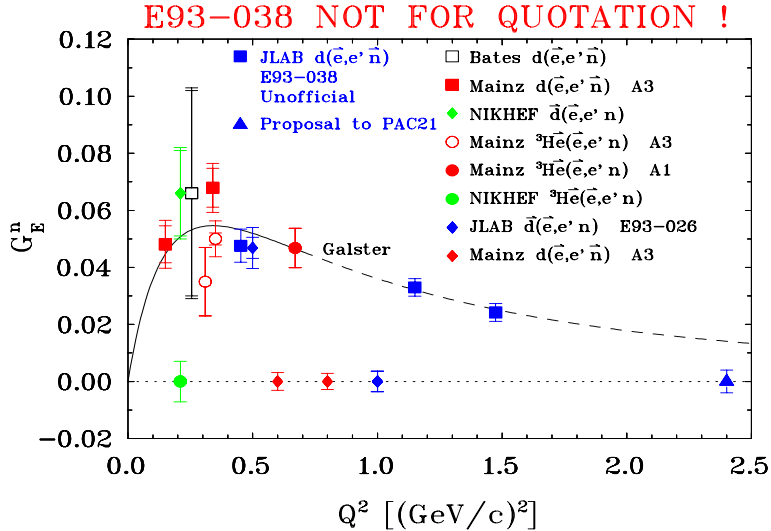


Figure 1:  $G_E^n$  versus  $Q^2$ . The line reflects the Galster parameterization of  $G_E^n$ .

Recently, Schiavilla and Sick (2001) extracted values of  $G_E^n$  from analysis of  $t_{20}$  and  $T_{20}$  data on the deuteron, which were measured up to  $Q^2 \sim 1.7$  (GeV/c)<sup>2</sup>. The results are shown as circles in Fig. 2. The error bars include the spread of theoretical predictions and experimental uncertainties in the deuteron quadrupole form factor. These results are consistent also with the Galster parameterization. The preliminary results from the E93-038 measurements are plotted as squares also in Fig. 2 with error bars that are significantly smaller than those extracted by Schiavilla and Sick from the deuteron quadrupole form factor.

Polarization measurements of  $G_E^n$  at  $Q^2$  above  $\approx 1$  (GeV/c)<sup>2</sup> require the beam energies available at CEBAF. In the technique demonstrated in E93-038 with a high-luminosity, high-efficiency polarimeter and a dipole magnet ahead of the polarimeter to precess the spin of the neutron, we measured the ratio of two neutron scattering asymmetries: one asymmetry from

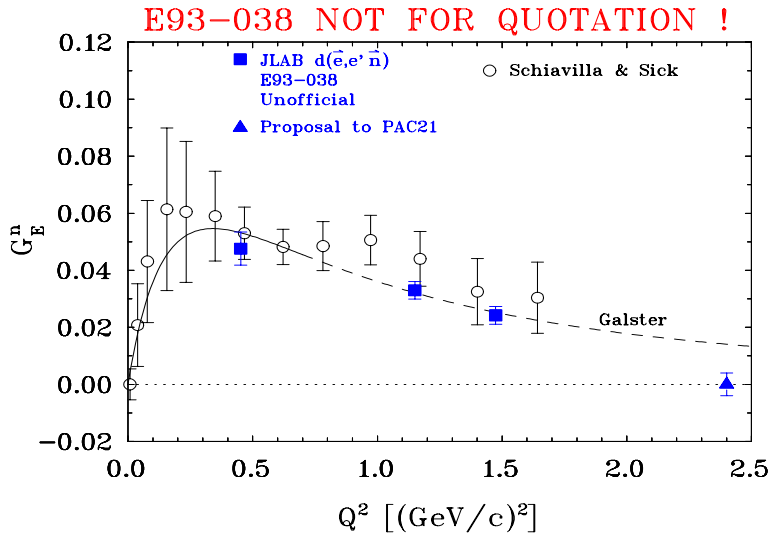


Figure 2:  $G_E^n$  data extracted from the deuteron quadrupole form factor by Schiavilla and Sick (open circles) together with the results of JLab E93-038 preliminary measurements (filled squares).

precessing the neutron polarization vector in a positive direction; the other, from precessing in a negative direction. In this ratio technique, systematic uncertainties are small because the analyzing power cancels in the ratio, and the beam polarization cancels also because, as demonstrated in E93-038, the beam polarization does not change much during the sequential measurements of the scattering asymmetries.

In the high  $Q^2$  region above  $1.5 \text{ (GeV/c)}^2$ , our present knowledge of the electric and magnetic form factors  $G_E$  and  $G_M$  for neutrons was obtained from measurements of the angular dependence of the cross section by quasielastic electron-deuteron scattering. Subtraction of the contribution from the proton in the deuteron introduces a large uncertainty. These previous experiments contain large systematic errors because of uncertainties in the theoretical description of the deuteron, mostly from final-state interactions (FSI) and meson-exchange currents (MEC). In the  $Q^2$  region from  $1.75$  to  $4.00 \text{ (GeV/c)}^2$ , Lung et al. (1993) reported measurements from SLAC-NE11 of quasielastic e-d cross sections at forward and backward angles which permit Rosenbluth separation of  $G_E^n$  and  $G_M^n$  at  $Q^2 = 1.75, 2.50, 3.25,$  and  $4.00 \text{ (GeV/c)}^2$ . The data of Lung et al. (1993) for  $(G_E^n/G_D)^2$  are plotted in Fig. 3 as a function of  $Q^2$ . Also plotted in Fig. 3 is the Galster parameterization. The error bars from JLab E93-038 are much smaller than those from SLAC-NE11. Although Lung et al. (1993) stated that their  $G_E^n$  data from SLAC-NE11 were consistent with  $(G_E^n)^2 = 0$  for  $1.75 < Q^2 \text{ (GeV/c)}^2 < 4.00$ , these data appear consistent also with the Galster parameterization. The NE11 error bars do not permit distinguishing between  $(G_E^n)^2 = 0$  and the Galster parameterization.

*The correct  $Q^2$ -dependence of  $G_E^n$  above  $1.5 \text{ (GeV/c)}^2$  remains in doubt. We need to know whether  $G_E^n$  will continue to follow the Galster parameterization above  $Q^2 = 1.5 \text{ (GeV/c)}^2$ , or whether  $G_E^n$  will approach zero or even become negative. There is no theoretical reason for  $G_E^n$  to follow the Galster parameterization at high  $Q^2$  values. The parameterization of Galster et al. (1971) for  $G_E^n$  was based on the best fit to the experimental data available on electron-*

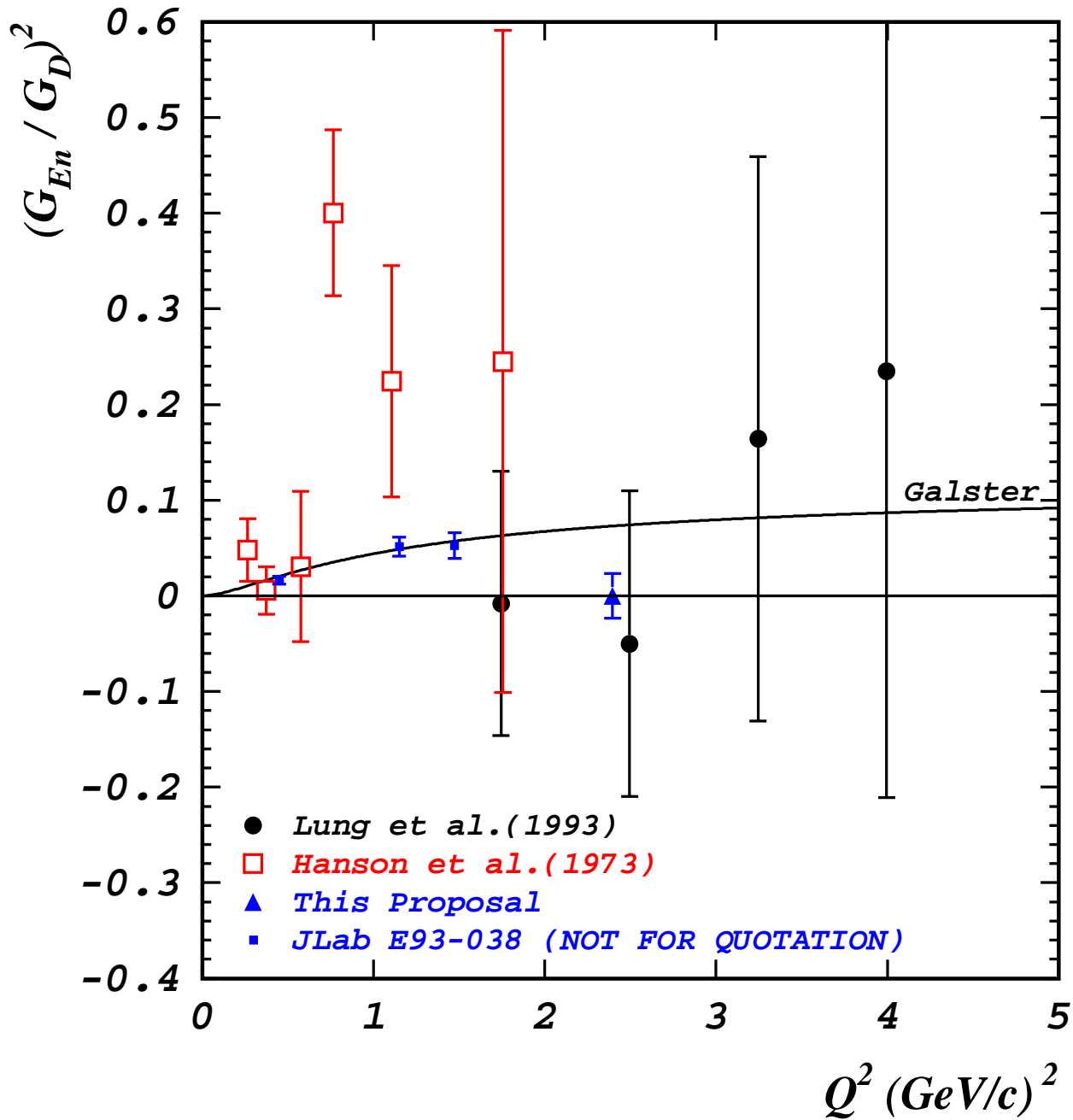


Figure 3:  $(G_{En}^n / G_D)^2$  as a function of  $Q^2$ . The data plotted as filled circles are from SLAC-NE11 [Lung et al. (1993)]; the data plotted as open squares are from Hanson et al. (1973). The solid line is the Galster parameterization. The uncertainty projected in this proposal for  $Q^2 = 2.40$   $(\text{GeV}/c)^2$  is for a value  $(G_{En}^n / G_D)^2 = 0.0365$ , which is one-half of the Galster value. The filled squares are data from E93-038.

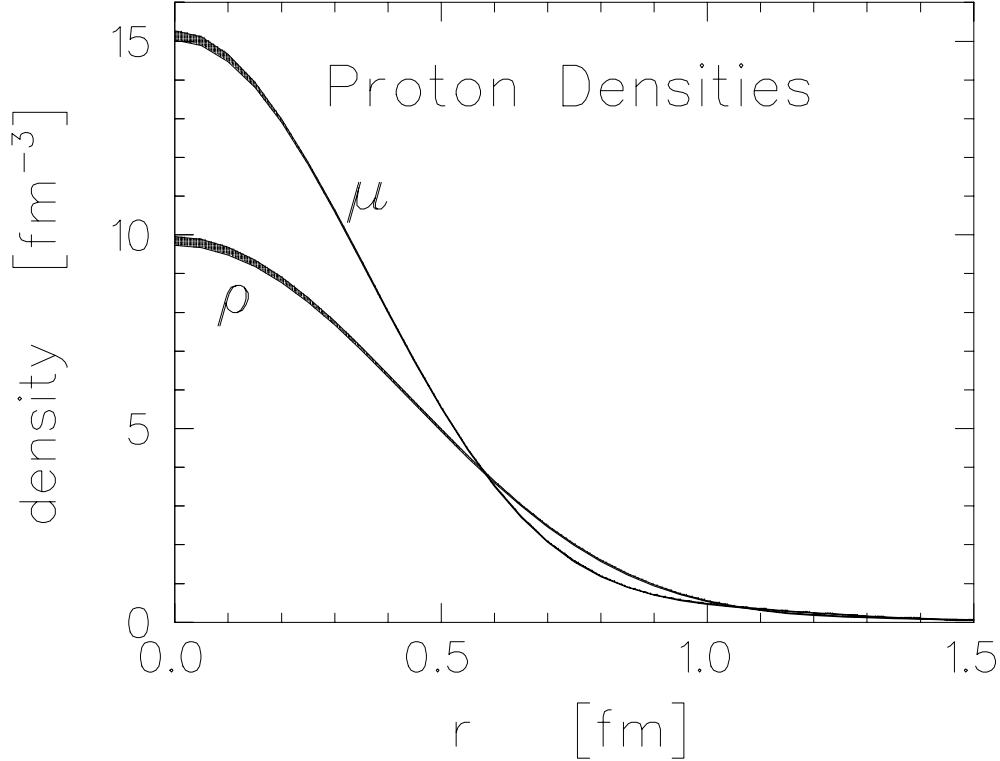


Figure 4: Comparison between fitted charge ( $\rho$ ) and magnetization ( $\mu$ ) densities for the proton. The error bands are tight and difficult to discern.

deuteron scattering up to  $Q^2 \sim 0.7$  (GeV/c)<sup>2</sup>. The best fit was found with the wave function of Feshbach and Lomon (1967). Our technique permits us to extend the measurements of  $G_E^n$  to the  $Q^2$  region up to about 2.5 (GeV/c)<sup>2</sup>. *In contrast to the Rosenbluth separation method, the polarization transfer method proposed here permits an experimental determination of the sign of  $G_E^n$ . This ability is another nice feature of the polarization transfer technique — especially in view of the fact that nothing is known about the sign of  $G_E^n$  at high  $Q^2$ .* Here we propose to measure  $G_E^n$  at  $Q^2 = 2.4$  (GeV/c)<sup>2</sup> with sufficient accuracy to challenge rigorous Lattice QCD calculations.

## 1.2 Improved Precision of Interior Charge Density

The measurement of  $G_E^n$  at  $Q^2 = 2.4$  (GeV/c)<sup>2</sup> will better define the short distance behavior of the wave function. The dependence of  $G_E^n$  on  $Q^2$  reflects the radial distribution of charge density in the neutron. The measurement of  $G_E^n$  at  $Q^2 = 2.4$  (GeV/c)<sup>2</sup> will reduce the *incompleteness error* in extracting the radial distribution of the charge density in the neutron. To properly extract the radial distribution of the charge density, it is necessary to have a theory with relativistic corrections. Appendix A is a preprint by Kelly (2001b) that uses a boost correction for the relationship between densities in the nucleon rest frame to those in the Breit frame to extract nucleon charge and magnetization densities from data on Sachs form factors.  *$G_E^n$  data at higher  $Q^2$  are needed to improve the interior ( $r = 0$ ) precision of the neutron charge density.* Kelly’s preprint uses only published data; the results for the charge and magnetization densities

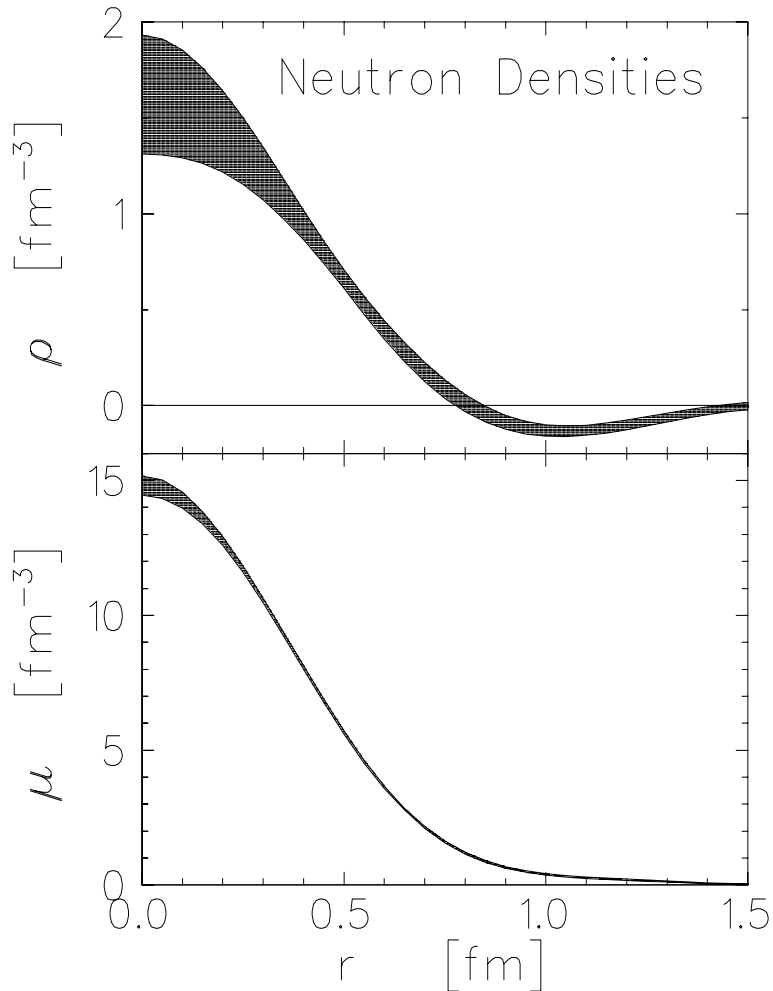


Figure 5: Charge ( $\rho$ ) and magnetization ( $\mu$ ) densities for the neutron.

are shown in Fig. 4 for the proton and in Fig. 5 for the neutron. *The uncertainty in the interior ( $r = 0$ ) charge density is less than one percent for the proton and very much larger ( $\sim 19\%$ ) for the neutron.*

Figure 6 shows the sensitivity to two possible outcomes of the proposed measurement at  $2.4 \text{ (GeV}/c)^2$ . Kelly (Private Communication, 2001) extracted the neutron charge density from a fit to the preliminary E93-038 data, all other polarization data, and the data extracted by Schiavilla and Sick (2001) on  $G_E^n$  versus  $Q^2$ . *He used a Fourier-Bessel expansion (FBE) to provide a more general parameterization than the simple two-parameter Galster fit.* The FBE minimizes model bias and facilitates analysis of the uncertainty in the extracted charge density. Also, he used a relativistic relationship between the Sachs form factor  $G_E(Q^2)$  and the Fourier transform of the charge density in the nucleon rest frame:  $G_E(Q^2) = \tilde{\rho}_{ch}(k^2)$ . The internal spatial frequency (or wave number)  $k$  is related to the invariant momentum transfer by  $k^2 = Q^2/(1+\tau)$ . This invariant relativistic relation is based on the relativistic Skyrmion model of Ji (1991). Figure 6 compares the FBE analysis with the two-parameter Galster parameterization. Figure 6 contains nine panels. The first panel contains the existing data. Both the FBE and Galster give comparable fits to the data; however, *note that the FBE falls faster than Galster above*

## Sensitivity to High $Q^2$

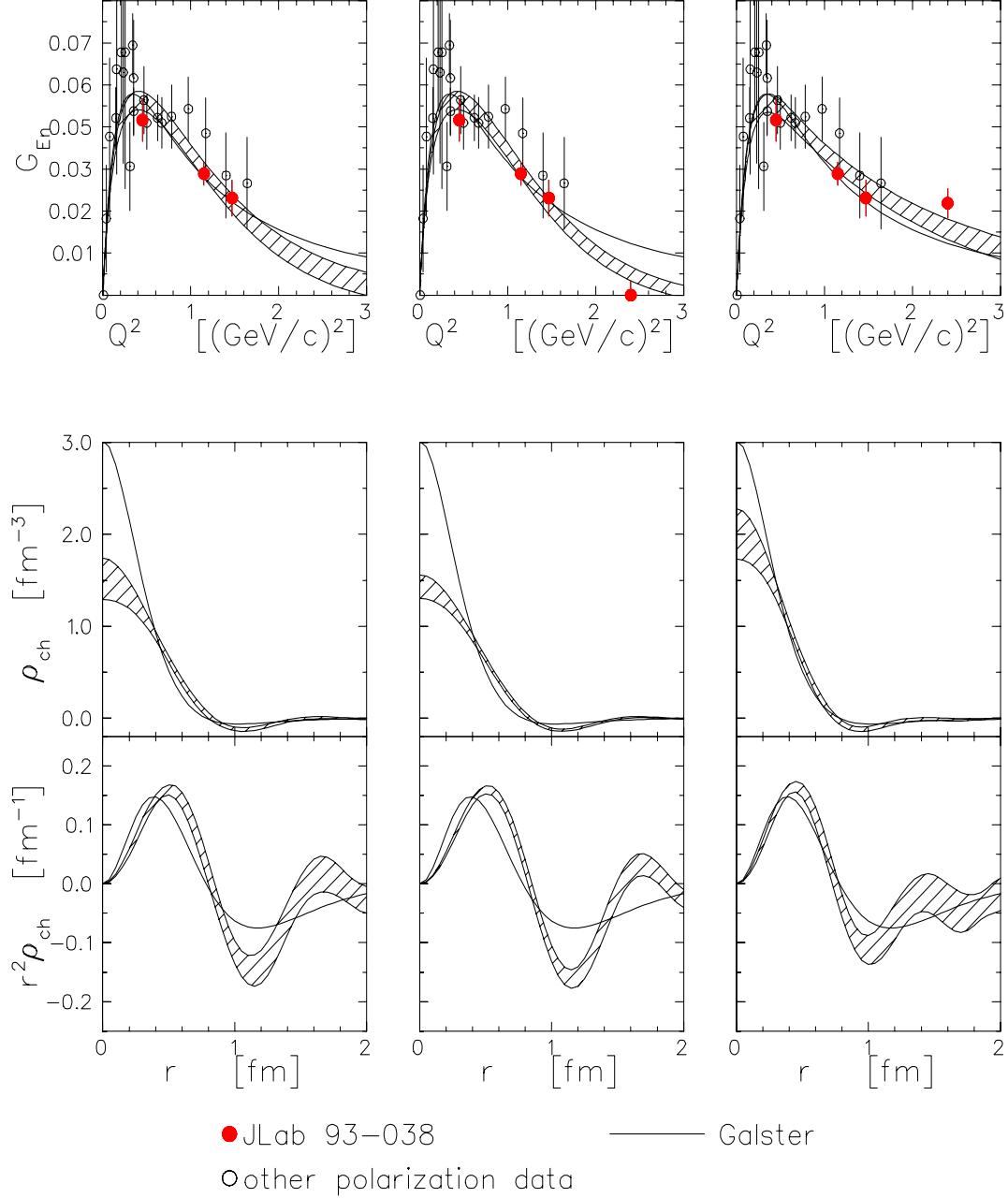


Figure 6: Comparison of the FBE analysis of  $G_E^n$  data with the two-parameter Galster parameterization. *The more general FBE parameterization permits more latitude in the extrapolation of the data to higher  $Q^2$ .*

our highest  $Q^2$  point at  $1.47 \text{ (GeV/c)}^2$ . The second panel assumes a measurement at  $Q^2 = 2.4 \text{ (GeV/c)}^2$  that falls just below the error band projected by the data in the first panel; the third panel assumes a measurement at  $Q^2 = 2.4 \text{ (GeV/c)}^2$  that falls just above the Galster parameterization. The next three panels show radial distributions of the charge density  $\rho_{ch}$ . As seen in the fourth panel, the uncertainty near the origin becomes smaller ( $\sim 14\%$ ), as expected, when the preliminary data from E93-038 are included. If the proposed measurement at  $Q^2 = 2.4 \text{ (GeV/c)}^2$  yields a small  $G_E^n$  value (close to the form factor band projected by the data), the uncertainty in the interior charge density is reduced further (to  $\sim 6\%$ ); alternatively, if the proposed measurement yields a large  $G_E^n$  value somewhat above the Galster value, the fitted FBE density moves toward Galster and increases the interior density (to  $\sim 12\%$ ), which is still smaller than the 14% without the measurement at  $Q^2 = 2.4 \text{ (GeV/c)}^2$ . The widening of the interior band occurs in this case probably because the form factor falls more slowly, which affects the interior density. The Galster parameterization shows a much higher density near the origin than the FBE. The last three panels reveal differences between the FBE and Galster in the radial distribution of  $r^2\rho_{ch}$ . The peak in  $r^2\rho_{ch}$  versus  $r$  comes earlier for Galster, and Galster has a more extended outer lobe. In all panels in Fig. 6, the shaded band of the FBE represents the uncertainty envelope. The multiplicative factor  $r^2$  enhances the visibility of the negative lobe. *The interior charge density will be sensitive to the measurement at  $Q^2 = 2.4 \text{ (GeV/c)}^2$ .*

Isgur (1998) noted that the interpretation of the neutron's electric form factor within many models has been obscured by relativistic effects. He demonstrated that, to leading order in the relativistic expansion of a constituent quark model, the Foldy term cancels exactly against a contribution to the Dirac form factor  $F_1$  to leave intact the naive interpretation of  $G_E^n$  as arising from the neutron's rest frame charge distribution.

### 1.3 Better Knowledge of Neutron Structure

*Any model based on Quantum Chromodynamics (QCD) must be able to predict nucleon and pion form factors correctly.* QCD models that are used to calculate nucleon form factors include the following: The relativistic constituent quark model (RCQM) [Chung and Coester (1991), Aznaurian (1993), Frank, Jennings, and Miller (1996)], the di-quark model [Kroll, Schurmann, and Schweiger (1992)], QCD sum rules [Radyushkin (1984)], and the cloudy bag model [Lu, Thomas, and Williams (1998)]. Recent results from JLab E93-027 on  $G_E^p$  motivated RCQM calculations [Pace et al. (2000), De Sanctis et al. (2000), Cardarelli and Simula (2000)]. These recent RCQM calculations reproduce the data of E93-027 when relativistic effects, which were omitted from previous calculations, are included.

Holzwarth (1996) found that a chiral soliton model could reproduce the essential features of nucleon form factors over three orders of magnitude in  $Q^2$ . The three basic ingredients in the soliton model of Holzwarth are: (1) an extended object (the standard skyrmion), (2) partial coupling to vector mesons in both isospin channels, and (3) relativistic recoil corrections. The soliton model of Holzwarth describes the  $G_E^p$  data from JLab E93-027 and E99-007, which are plotted in Fig. 7a. The heavy solid line in Fig. 7a is the soliton model of Holzwarth with the same value of the model parameter ( $\lambda_0 = \lambda_1 = 0.75$ ) for isoscalar and isovector mesons. The shape of the  $G_E^n$  curve (in Fig. 2 of the article by Holzwarth) is similar to the Galster parameterization, but the absolute values of  $G_E^n$  are higher by nearly a factor of two; in his paper, Holzwarth states that the absolute values can be reduced by allowing the adjustable parameter  $\lambda$  in the model

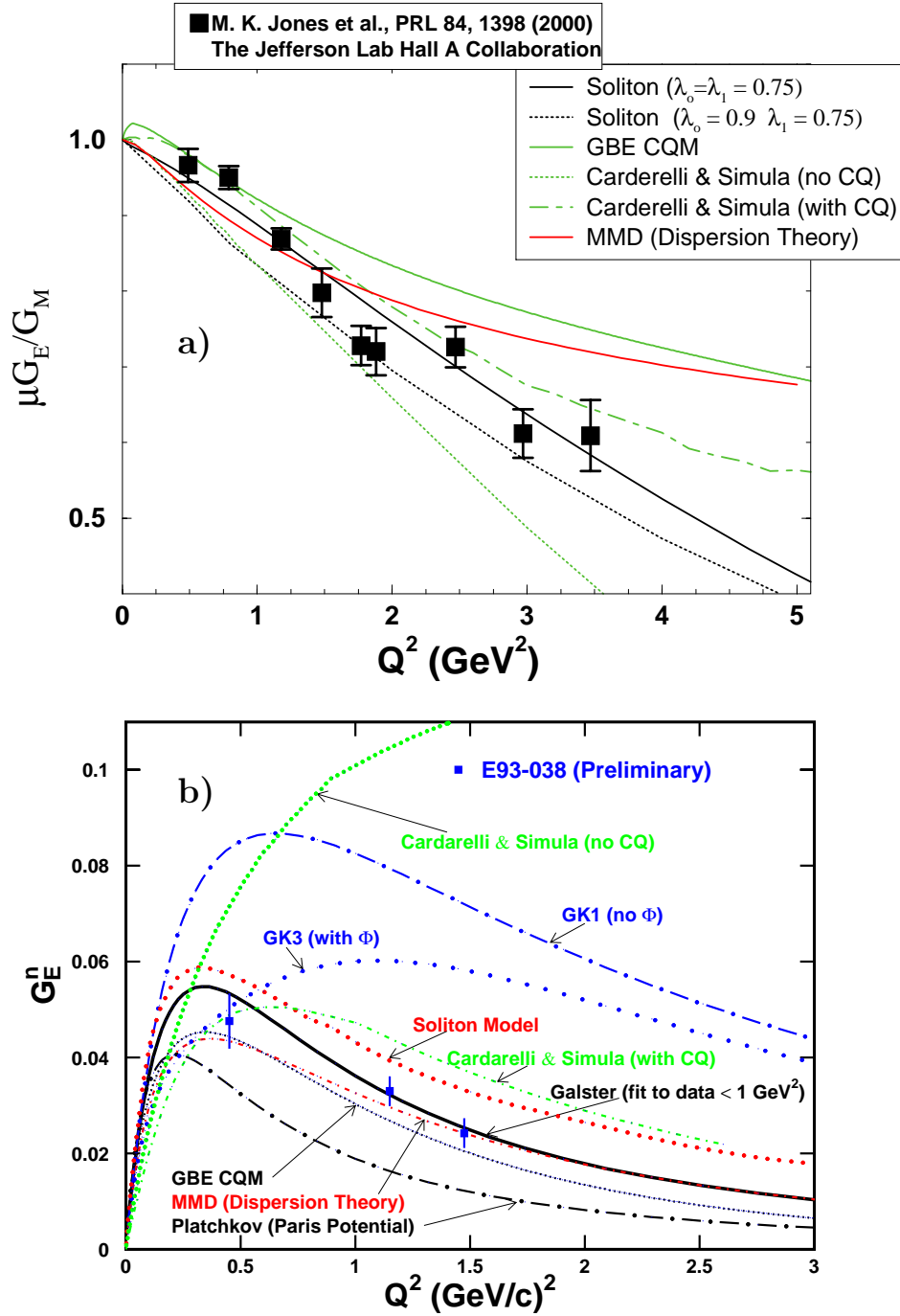


Figure 7: Some model predictions for  $G_E^p$  (panel a) and  $G_E^n$  (panel b).

to differ slightly for isoscalar ( $\lambda_0$ ) and isovector ( $\lambda_1$ ) mesons. Responding to a request from the principal investigator, Holzwarth used different values of the model parameter ( $\lambda_0 = 0.9$  and  $\lambda_1 = 0.75$ ) for isoscalar and isovector mesons in order to lower the prediction for  $G_E^n$ ; however, with these values, the  $G_E^p$  prediction falls below the data, as seen by the dotted black curve in Fig. 7a. Also, the  $G_E^n$  prediction still lies above the data, as seen by the dotted soliton model curve in Fig. 7b.

Figure 7b shows some model predictions for  $G_E^n$  versus  $Q^2$ . Existing data [below  $\approx 0.7$  (GeV/c)<sup>2</sup>] reject the Gari-Krumpelmann (1985) model GK1 (no  $\Phi$ ). Our data from E93-038 reject another Gari-Krumpelmann (1992) model GK3 (with  $\Phi$ ) and the Platchkov (1990) parameterization with the Paris potential. Gari and Krumpelmann (1992) reanalyzed the electromagnetic form factor data of the nucleon with emphasis on the neutron electric form factor. They showed that strange quark contributions can reduce the neutron electric form factor at low  $Q^2$  with little effect on the other nucleon form factors. The model of Mergell, Meissner, and Drechsel (MMD) (1996) gives a result similar to Galster above  $Q^2 \approx 0.7$  (GeV/c)<sup>2</sup>; however, it falls below Galster in the  $Q^2$  region around the peak, and it does not agree with the  $G_E^p$  data as seen in Fig. 7a. The Goldstone-Boson-Exchange-Constituent-Quark Model [GBE CQM] of Wagenbrunn et al. (2001) falls below  $G_E^n$  data from E93-038, and the RCQM of Cardarelli and Simula lie above the  $G_E^n$  data. *It appears that no model predicts both  $G_E^n$  and  $G_E^p$  data !!*

Negele (2000) is leading a major effort to use lattice QCD to understand the structure and interaction of hadrons. Fundamental lattice calculations will become available to solve QCD, the field theory of quarks and gluons. Currently, lattice calculations are limited by computer power; however, more computing power is expected to be available soon. Lattice QCD calculations are fundamental, whereas various model calculations are not. Lattice QCD has made impressive strides recently, with rigorous methods for separating hard and soft contributions and recent methods for extrapolation to the chiral limit for light quarks using explicit representations of nonanalytic contributions.

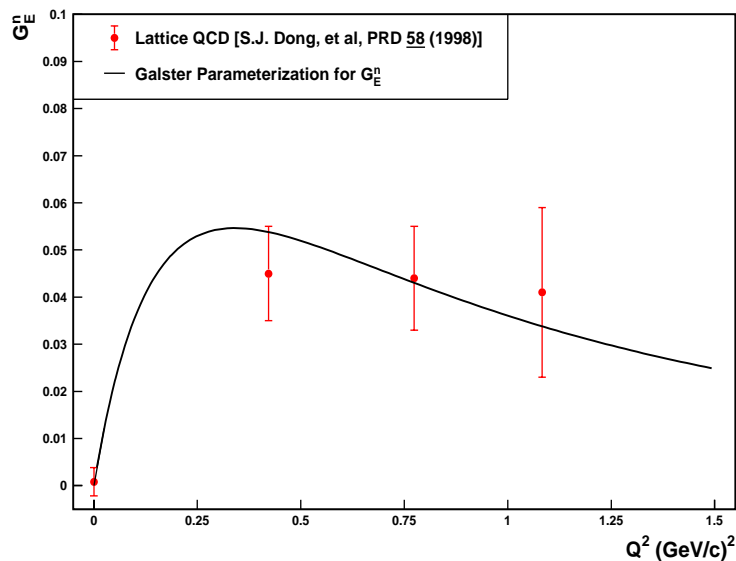


Figure 8: Lattice QCD calculation result for  $G_E^n$ .

Dong et al. (1998) and Liu (2001) reported a lattice QCD calculation of  $G_E^n$  in connection with their investigation of the strangeness magnetic moment of the nucleon. The results [from Fig. 5(b) of Dong et al. (1998)] are compared to the Galster parameterization in Fig. 8. Liu (2001) states that the errors are getting too big to make a useful prediction above  $Q^2 \approx 1.3$  (GeV/c)<sup>2</sup>. Liu (2001) states that the next generation of calculations may reach  $Q^2 = 2.4$  (GeV/c)<sup>2</sup>. Dong et al. (1998) state that future calculations are needed to investigate the systematic errors associated with the finite volume and lattice spacing as well as with the quenched approximation.

## 1.4 Better Understanding of Electron Scattering Data From Nuclei

In their paper on electron scattering off nuclei, Drechsel and Giannini (1989) state (on page 1109) that “All calculations of nuclear electromagnetic properties suffer from the poor knowledge of  $G_E^n$ .”

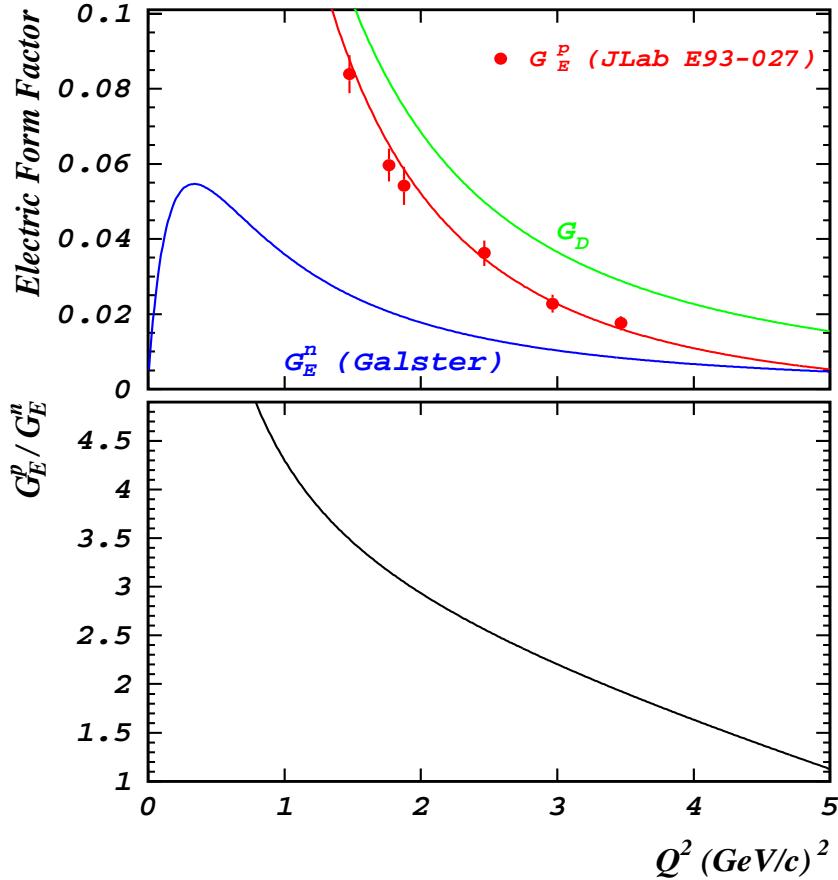


Figure 9: Proton and neutron form factors as a function of  $Q^2$ . The red solid line in the top panel is a parameterization from Eq. (4) for  $G_E^p$ .

As  $Q^2$  increases, the values of  $G_E^p$ , the electric form factor of the proton, approach the values of  $G_E^n$ , represented by the Galster parameterization. Plotted in Fig. 9 as a function of  $Q^2$  are the neutron electric form factor for the Galster parameterization, the proton electric form factor

for the dipole parameterization, and the proton electric form factor points measured in JLab E93-027. The Galster parameterization for  $G_E^n$  is:

$$G_E^n = -\tau(1 + 5.6\tau)^{-1}G_M^n, \quad (\text{Galster}) \quad (1)$$

with

$$G_M^n = -1.91(1 + Q^2/0.71)^{-2}, \quad (\text{Dipole}) \quad (2)$$

and

$$\tau = Q^2/4M^2. \quad (3)$$

The measured  $G_E^p$  points have been fitted with the following parameterization:

$$G_E^p = G_D [1 - 0.14(Q^2 - 0.30)], \quad (\text{Fit to Hall A FPP Measurements}) \quad (4)$$

with

$$G_D \equiv (1 + Q^2/0.71)^{-2}. \quad (\text{Dipole}) \quad (5)$$

The magnitude of  $G_E^n$  is not insignificant compared to  $G_E^p$  in the  $Q^2$  region above about  $2 \text{ (GeV}/c)^2$ . The ratio of  $G_E^p$  (E93-027) to  $G_E^n$  (Galster) is plotted in the bottom panel of Fig. 9. The  $G_E^p$  data measured in E93-037 turned out to be a *surprise* – falling faster with  $Q^2$  than expected from the global analysis of earlier SLAC data. The nature of the decrease of  $G_E^n$  with  $Q^2$  may be a surprise also.

*Because the isovector electric form factors of nuclei are proportional to the difference  $G_E^p - G_E^n$  (and the isoscalar electric form factors are proportional to the sum  $G_E^p + G_E^n$ ), the value of  $G_E^n$  is needed for the understanding of electron scattering experiments that probe electric structure functions at high momentum transfer.* The ratio of the isoscalar cross section to the isovector cross section depends sensitively on the value of  $G_E^n$ :

$$\frac{\sigma_{\text{isoscalar}}}{\sigma_{\text{isovector}}} = \left( \frac{G_E^p + G_E^n}{G_E^p - G_E^n} \right)^2. \quad (6)$$

This ratio is plotted in Fig. 10 as a function of  $Q^2$ . This ratio is unity if  $G_E^n = 0$ ; however, this ratio is about five at  $Q^2 = 2.4 \text{ (GeV}/c)^2$  if  $G_E^n$  continues to follow the Galster parameterization and if  $G_E^p$  follows Eq. (4). A better knowledge of  $G_E^n$  is needed for the interpretation of electron scattering from nuclei at high momentum transfer. This knowledge is needed for the analysis of few-body data near  $Q^2 = 2.4 \text{ (GeV}/c)^2$ , which is right in the middle of the  $Q^2$  range for all few-body measurements at Jefferson Lab. With an uncertainty  $\Delta G_E^n \approx 0.004$ , we will be able to distinguish between  $G_E^n = 0$  and Galster [ $G_E^n = 0.014$  at  $Q^2 = 2.4 \text{ (GeV}/c)^2$ ].

## 2 Theoretical Background

Arenhoevel (1987) calculated the effect of the electric form factor of the neutron  $G_E^n$  on the polarization transfer in the  $d(\vec{e}, e'\vec{n})p$  reaction in the quasifree region, where the deuteron serves as a neutron target while the proton acts mainly as a spectator. Using a nonrelativistic theory

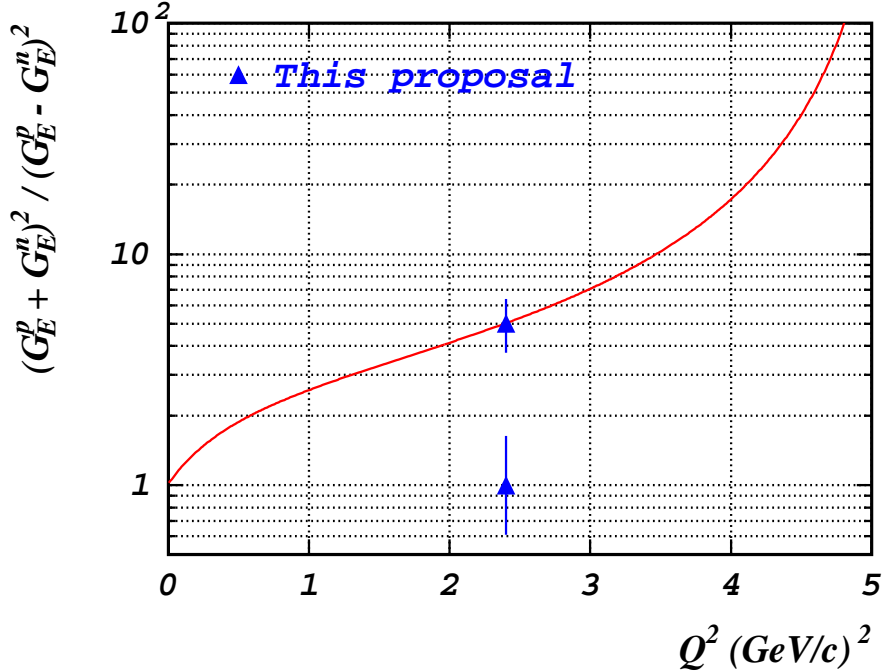


Figure 10: The ratio of isoscalar and isovector cross-sections [Eq. (6)] as a function of  $Q^2$ . We assume the Galster parameterization for  $G_E^n$  [Eq. (1)] and the parameterization from Eq. (4) for  $G_E^p$ . The error bars for the presented points originate from the projected uncertainty  $\Delta G_E^n = 0.0042$  and the uncertainty of the E93-027 measurement at  $Q^2 = 2.47$  ( $\text{GeV}/c$ )<sup>2</sup> ( $\mu_p g_p = 0.726 \pm 0.027 \pm 0.062$ ).

and a realistic nucleon-nucleon potential, Arenhoevel found that the sideways polarization of the recoil neutron  $P_{S'}$ , which vanishes for coplanar kinematics and unpolarized electrons, is most sensitive to  $G_E^n$  for neutron emission along the momentum-transfer direction in the quasifree case. Using the parameterization of Galster et al. (1971) for  $G_E^n$ , Arenhoevel's calculation indicates that even away from the forward-emission direction (with respect to the direction of the momentum transfer  $\vec{q}$ ), the increase in the sideways polarization of the neutron  $P_{S'}$  is small for  $G_E^n = 0$ , but increases when  $G_E^n$  is switched on, and that this increase prevails up to a neutron angle of nearly  $30^\circ$  measured with respect to  $\vec{q}^{c.m.}$  in the center-of-mass system. In the forward direction with respect to  $\vec{q}^{c.m.}$ , Arenhoevel found also that the neutron polarization  $P_{S'}$  is insensitive to the influence of final-state interactions (FSI), meson-exchange currents, and isobar configurations, and that this lack of sensitivity holds again up to an angle of nearly  $20^\circ$  away from the forward direction with respect to  $\vec{q}^{c.m.}$ , which corresponds to a laboratory angle of about a few degrees away from the forward direction with respect to the  $\vec{q}^{lab}$ . Arenhoevel also studied the influence of different deuteron wave functions on the sideways neutron polarization  $P_{S'}$ . His results for quasifree kinematics (i.e., for neutron emission along  $\vec{q}$ ) show almost no dependence on the deuteron model. The Arenhoevel calculation shows that dynamical uncertainties are very small. Finally, Beck and Arenhoevel (1992) investigated the role of relativistic effects in electrodisintegration of the deuteron for quasifree kinematics. They found that the dependence on the parameterization of the nucleon current in terms of Dirac-Pauli or Sachs form factors is reduced considerably by inclusion of the relativistic contributions.

Rekalo, Gakh, and Rekalo (1989) used the relativistic impulse approximation to describe the polarization effects sensitive to  $G_E^n$  in deuteron electrodisintegration. In the deuteron quasielastic peak, the neutron polarizations calculated in the relativistic approach agree with the results of Arenhoevel (1987). A later study by Mosconi, Pauschenwein, and Ricci (1991) of nucleonic and pionic relativistic corrections in deuteron electrodisintegration does not change the results of Arenhoevel. Laget (1990) investigated the effects of nucleon rescatterings and meson-exchange currents on the determination of the neutron electric form factor in the  $d(\vec{e}, e'\vec{n})p$  reaction. He concluded that the measurements of the sideways polarization of the neutron appears to be the most direct way to determine the neutron electric form factor. He concluded also that in quasifree (colinear) kinematics, the neutron polarization in the exclusive reaction is equal to the value expected in the elementary reaction  $n(\vec{e}, e'\vec{n})$  and that corrections from final-state interactions and meson-exchange currents are negligible above  $Q^2 = 0.30$  (GeV/c)<sup>2</sup>, but that these corrections become sizeable below this momentum transfer; however, Herberg et al. (1999) found that (even in the quasifree peak) corrections for FSI in  $d(\vec{e}, e'\vec{n})p$  measurements at Mainz amounted to  $(8\pm 3)\%$  for  $Q^2 = 0.34$  (GeV/c)<sup>2</sup> and  $(65\pm 3)\%$  for  $Q^2 = 0.15$  (GeV/c)<sup>2</sup> of the value unperturbed by FSI. These corrections were based on the model of Arenhoevel et al. (1988). This correction is needed to account for the two-step process  $d(\vec{e}, e'\vec{p})n + d(\vec{p}, \vec{n})$  in the deuterium nucleus. In the second charge-exchange step, the sign of the polarization transferred to the neutron will be opposite to that from the primary  $d(\vec{e}, e'\vec{n})p$  process because the sign of the magnetic moment of the proton is opposite that of the neutron. This effect increases as the p-n charge exchange cross section increases in going to low  $Q^2$ .

## 3 Description of the Experiment

### 3.1 Experimental Arrangement

The experimental arrangement is shown in Fig. 11. A polarimeter detects the recoil neutron from the quasielastic  $d(\vec{e}, e'\vec{n})p$  reaction and measures the up-down scattering asymmetry from the projection of the polarization vector on the transverse axis. A dipole magnet (CHARYBDIS) in front of the polarimeter precesses the neutron polarization vector through an angle  $\chi$  to permit measurement of the scattering asymmetry  $\xi_+$  from the polarization vector component in the transverse (or sideways) direction. With another measurement of the scattering asymmetry  $\xi_-$  for a precession through an angle  $-\chi$ , the ratio of  $G_E$  and  $G_M$  is given by

$$g \equiv \left( \frac{G_E}{G_M} \right) = K_R \tan \chi \left( \frac{\eta + 1}{\eta - 1} \right), \quad (7)$$

where the asymmetry ratio

$$\eta \equiv \frac{\xi_-}{\xi_+} = \frac{P_-^x}{P_+^x}, \quad (8)$$

and  $K_R$  is a kinematic function that is determined by the electron scattering angle  $\theta_e$  in the  $d(\vec{e}, e'\vec{n})p$  reaction. For a total data-acquisition time  $T$ , the time fractions for measuring  $\xi_+$  and  $\xi_-$  are optimized to minimize the statistical uncertainty in  $g$ . The scattered electron from the

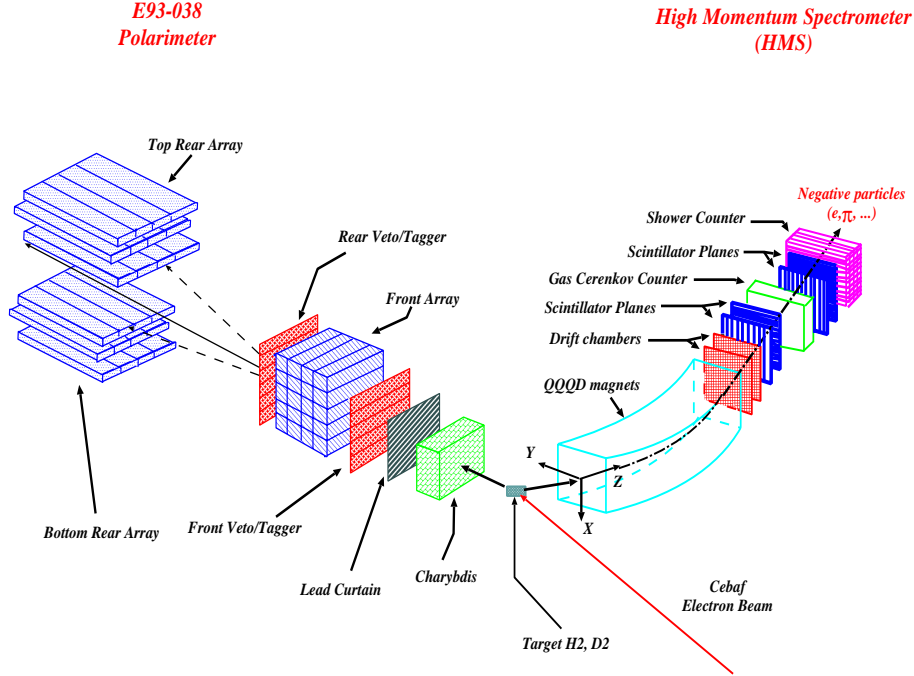


Figure 11: Schematic diagram of the experimental arrangement.

$d(\vec{e}, e' \vec{n})p$  reaction is detected with the high-momentum spectrometer (HMS) in coincidence with the recoil neutron.

In E93-038, the polarimeter consisted of 20 detectors in the front array and 12 detectors in each of two rear arrays for a total of 44 detectors. A double layer of veto/tagger detectors is located ahead of the front array, and another double layer of tagger detectors is located behind the front array. The configuration of this polarimeter was proposed by Madey (1995). To permit high luminosity, the dimensions of each of the 20 detectors in the front array were  $10 \text{ cm} \times 10 \text{ cm} \times 100 \text{ cm}$ , and the detectors in each rear array were shielded from the direct path of neutrons from the target. Compared to the configuration proposed originally for E93-038, this new configuration permitted doubling the height of the front array, thereby doubling the solid-angle acceptance of the neutron polarimeter. Doubling the neutron solid angle yields an increased electron-neutron coincidence rate. Figure 12 shows efficiencies and analyzing powers measured during E93-038 at JLab for events designated as “all neutrals”. The efficiency at each  $Q^2$  was extracted from the measured rate (events/mC) by inverting the count rate calculation. The analyzing power at each  $Q^2$  was extracted from the measured asymmetry and beam polarization. The “all neutrals” category includes both neutron elastic (n,n) scattering and charge-exchange (n,p) scattering from a proton in one of the scintillators of the front array. The inclusion of (n,p) events increases the polarimeter efficiency  $\epsilon$  but decreases the analyzing power  $A_Y$ ; however, the figure-of-merit  $A_Y^2 \epsilon$  for (n,n)+(n,p) events is larger than that for (n,n) events alone. Imposition of a cut on the recoil momentum reduces the efficiency, as can be seen in Fig. 12 by comparing the triangles and the circles. The curve labelled “KSU + SAID” was calculated with a combination of the KSU efficiency code (Cecil 1979) for the efficiency in the front and rear arrays and the SAID code (Arndt 1977, 2000) for estimating the angular distribution of the scattered nucleon.

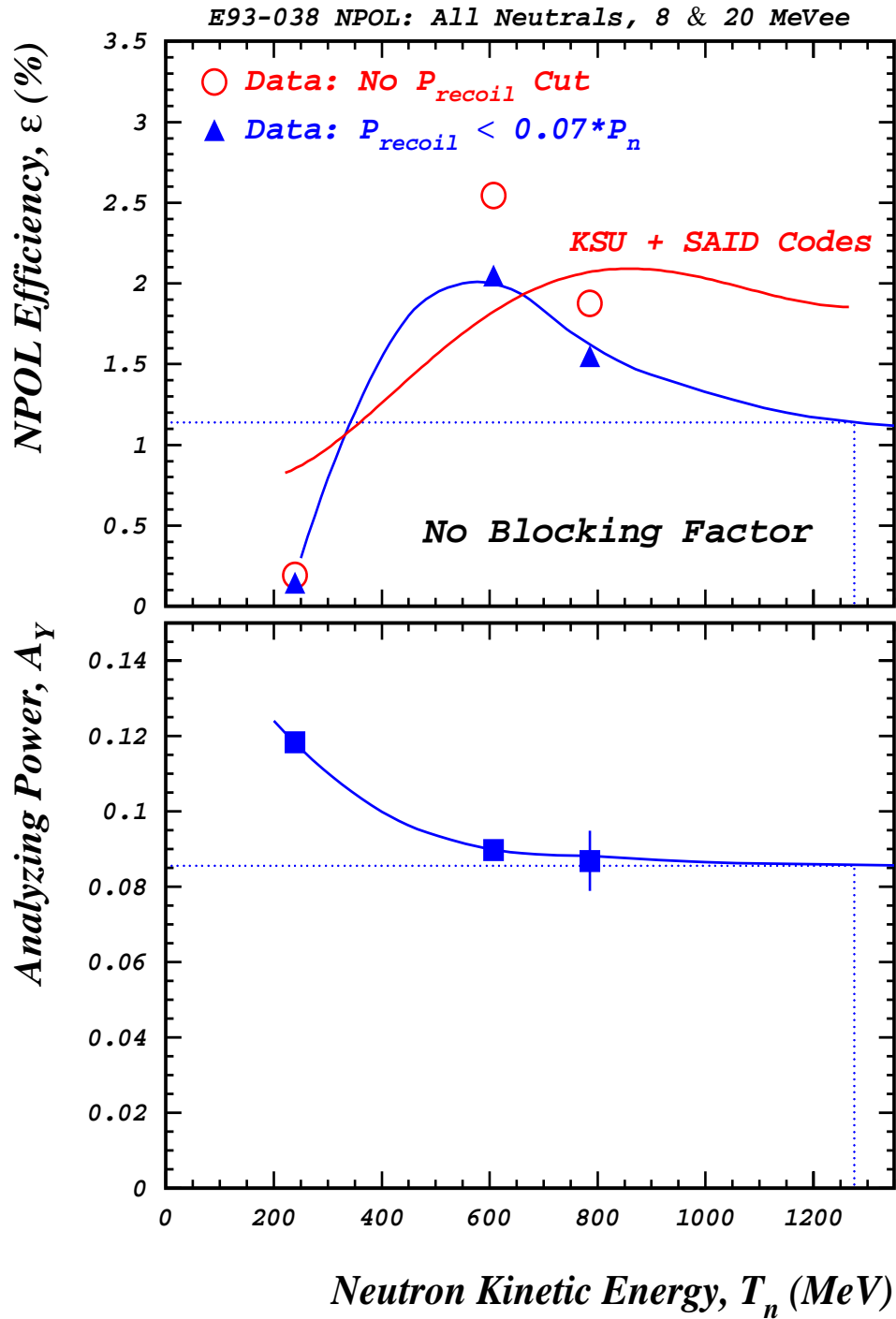


Figure 12: Efficiency (top panel) and the analyzing power (bottom panel) of the E93-038 neutron polarimeter. Data obtained during the E93-038 run.

**E = 0.884 GeV and a Charybdis Current of -170 A**

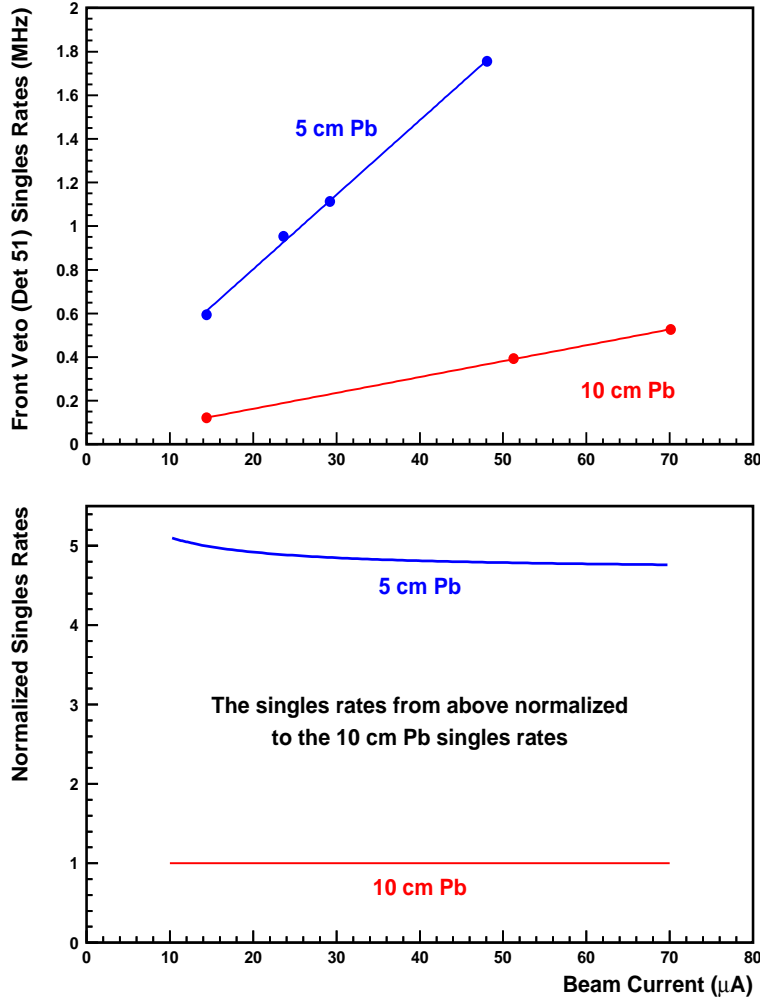


Figure 13: Singles rates for beam energy of 884 MeV and a CHARYBDIS current of -170 A.

The lead curtain ahead of the polarimeter is required to attenuate electromagnetic radiation and also to reduce the flux of charged particles incident on the polarimeter. The singles counting rate in one of the detectors decreases markedly when the thickness of the Pb increases from 5 cm to 10 cm; for example, the singles rates in one of the veto detectors (160 cm wide  $\times$  11 cm high  $\times$  0.64 cm thick) at a distance of about 6.7 m from a 15-cm LD<sub>2</sub> target are plotted in Fig. 13 as a function of the electron beam current at an energy of 884 MeV. For all beam currents, the singles rate is about five times higher with 5-cm Pb curtain. E93-038 used a 10-cm lead curtain in order to run at higher beam currents. We do not have data with a 5-cm lead curtain at higher beam energies. E93-038 ran with a 10-cm Pb curtain for all these energies. To measure the false asymmetry or the dilution of the asymmetry from the two-step process  ${}^2\text{H}(\vec{e}, e'\vec{p})_n + \text{Pb}(\vec{p}, \vec{n})$ , we acquire data with an LH<sub>2</sub> target.

*A significant advantage of this technique for measuring the ratio of the two scattering asymmetries is that the scale and systematic uncertainties are minimal because the relative uncertainty in the analyzing power of the polarimeter does not enter in the ratio. The same is true for the*

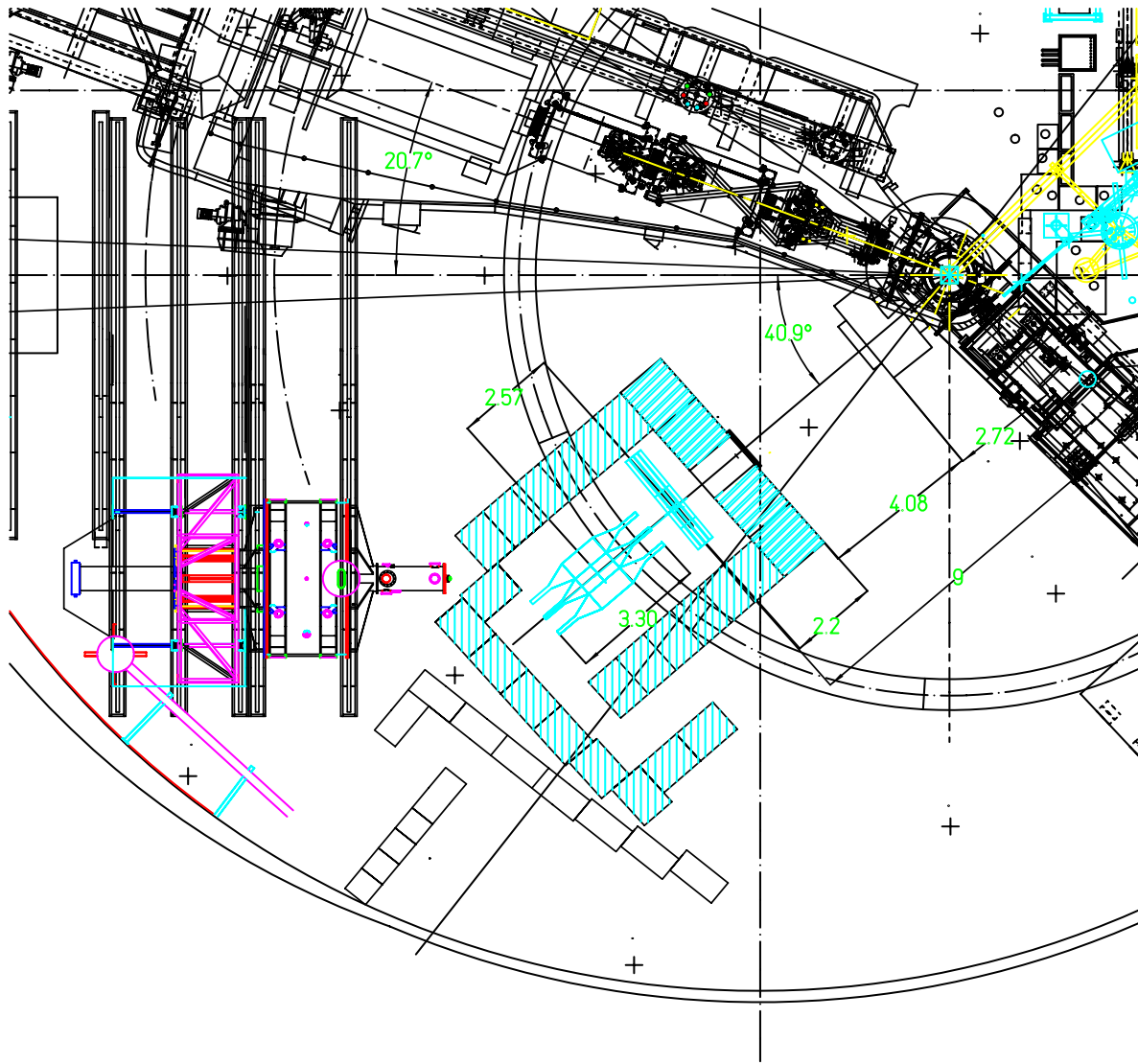


Figure 14: Footprint in Hall C of the polarimeter shielding enclosure for a neutron angle of 40.9 degrees and a mean flight path of 9.0 m. The shielding enclosure is compatible with the setup for the  $G_0$  experiment.

beam polarization  $P_L$  because, as demonstrated in E93-038,  $P_L$  does not change much during sequential measurements of  $\xi_+$  and  $\xi_-$ .

In the cross-ratio method of analysis of the scattering asymmetries measured in the polarimeter, Ohlsen and Keaton (1973) showed that false asymmetries cancel **to all orders** from helicity-dependent errors in charge integration or system dead-times, or from errors in detection efficiency and acceptances; and that false asymmetries cancel **to first order** from misalignments with respect to  $\vec{q}$ , or from a difference in the beam polarization for the two helicity states. The cross ratio is the ratio of two geometric means  $(N_U^+ N_D^-)^{1/2}$  and  $(N_U^- N_D^+)^{1/2}$ , where  $N_U^+(N_D^-)$  is the yield in the peak for neutrons scattered up(down) when the helicity was positive(negative).

In E93-038, we used the CHARYBDIS dipole magnet with an 8.25-inch gap and 2-inch field clamps. The 8.25-inch gap is large enough to fully illuminate the front detectors of our polarimeter (20-inch high by 40-inch wide). The precession angle  $\chi$  is the angle of rotation of the polarization vector measured with respect to the direction of motion of the particle in the rest frame of the particle after traversing the magnetic field. The neutron spin precession angle  $\chi$  is given by

$$\chi = -\frac{ge}{2M_p c \beta_n} \int B \Delta l = \frac{1.913e}{M_p c \beta_n} \int B \Delta l, \quad (9)$$

where  $g/2 = -1.913$ . The maximum central  $\int B \Delta l = 2.39$  Tm for CHARYBDIS with an 8.25-inch gap.

Figure 14 is a footprint in Hall C of the polarimeter shielding enclosure for a neutron angle of 40.9 degrees and a mean flight path of 9.0 m to the mid-plane of the front detector array in the polarimeter. This setup is compatible with the setup for the  $G_0$  experiment.

## 3.2 Kinematics

Four-Momentum Transfer, $Q^2$ (GeV/c) <sup>2</sup>	2.40
Beam Energy, $E_0$ (GeV)	5.00
Electron Scattering Angle, $\theta_e$ (deg)	20.70
Scattered Electron Momentum, $P_{e'}$ (GeV/c)	3.720
Neutron Scattering Angle, $\theta_n$ (deg)	40.9
Neutron Momentum, $P_n$ (GeV/c)	2.007
Neutron Kinetic Energy, $T_n$ (MeV)	1276
Neutron Velocity, $\beta_n$	0.906
Flight Path, $x$ (m)	9.0
Neutron Energy Resolution (HWHM), $\Delta T_n$ (MeV)	108
Field Integral to Precess Neutron Spin through 20 Degree, $B \Delta l$ (Tm)	0.5173
CHARYBDIS Current, $I$ (A)	127.5

Table 1: Kinematic conditions at a neutron scattering angle of 40.9° and a beam with a beam energy of 5.0 GeV. Also listed are the neutron energy resolution and the Charybdis field integral  $B \Delta l$  required to precess the neutron polarization vector through  $\pm 20$  degrees.

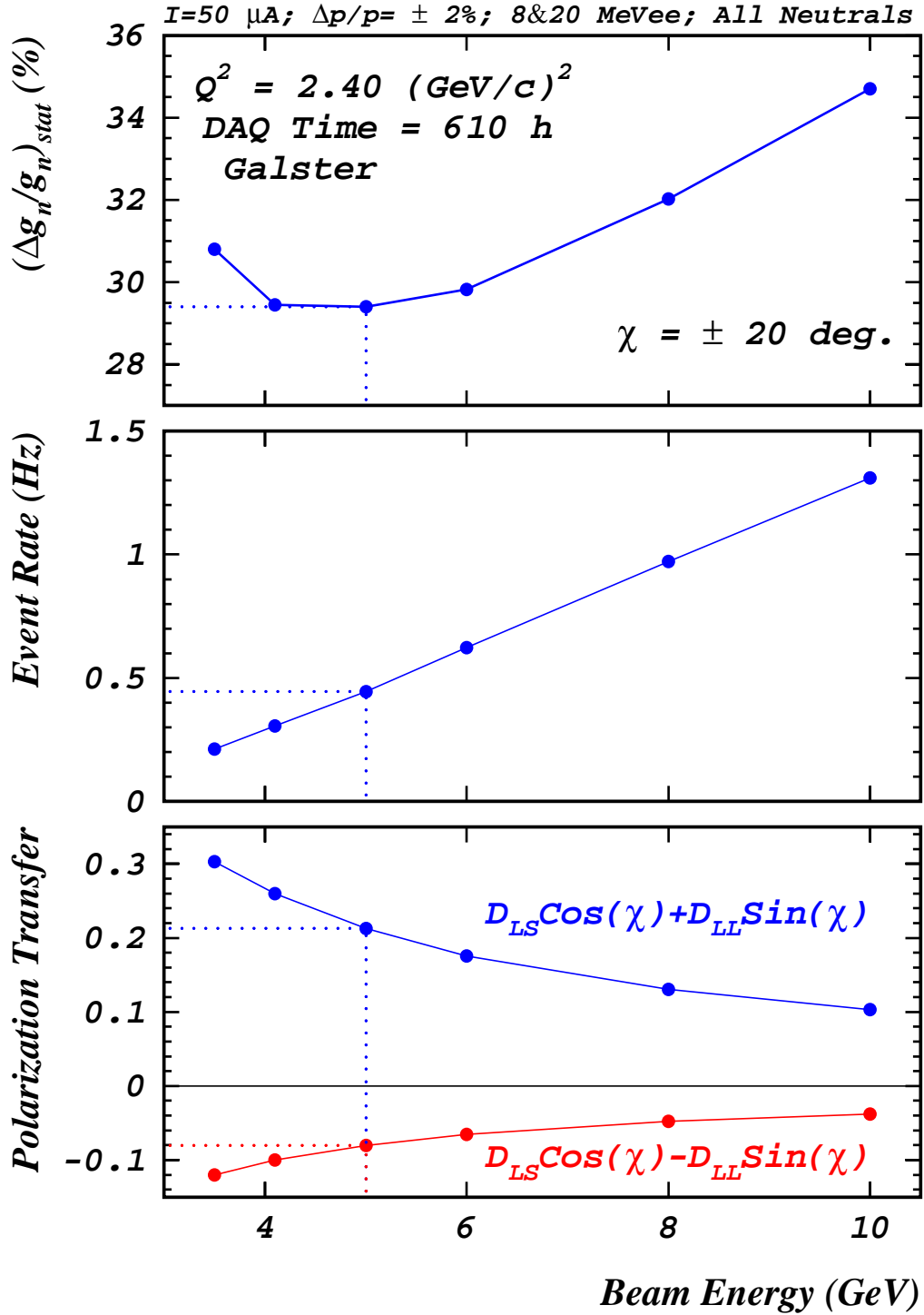


Figure 15: Statistical uncertainty, real event rate, and the polarization transfer, projected at  $Q^2 = 2.4 \text{ (GeV/c)}^2$ , as a function of beam energy. The statistical uncertainty increases for beam energies above  $\approx 5 \text{ GeV}$  because the polarization transfer at a fixed  $Q^2$  becomes smaller with increasing beam energy.

Table 1 lists the kinematics conditions, the  $B\Delta l$  required to precess the neutron polarization vector through  $\pm 20$  degrees, and the neutron energy resolution at a mean flight path of 9.0 m. The beam energy of 5.00 GeV was selected because it is in a region where the accelerator operates reliably (with fewer trips of the cavities), the experimental setup is compatible with the setup for the  $G_0$  experiment, and this beam energy results in a minimum or near-minimum statistical uncertainty, as seen in Fig. 15, for the Galster parameterization of  $G_E^n$ . The accelerator should be able to deliver a beam polarization of 75% at any energy. The range of reasonable angles of neutron spin precession is limited on the small-angle side by the requirement to have the magnetic field in CHARYBDIS strong enough to deflect a significant part of the quasielastic protons away from the front array of the polarimeter, and on the large-angle side by the fact that the statistical uncertainty  $\Delta g_n/g_n$  increases with precession angle  $\chi$ , as shown in Fig. 16. The precession angle  $\chi$  of  $20^\circ$  was chosen. Smaller precession angles were avoided because the smaller Charybdis current would reduce the deflection of protons away from the front array.

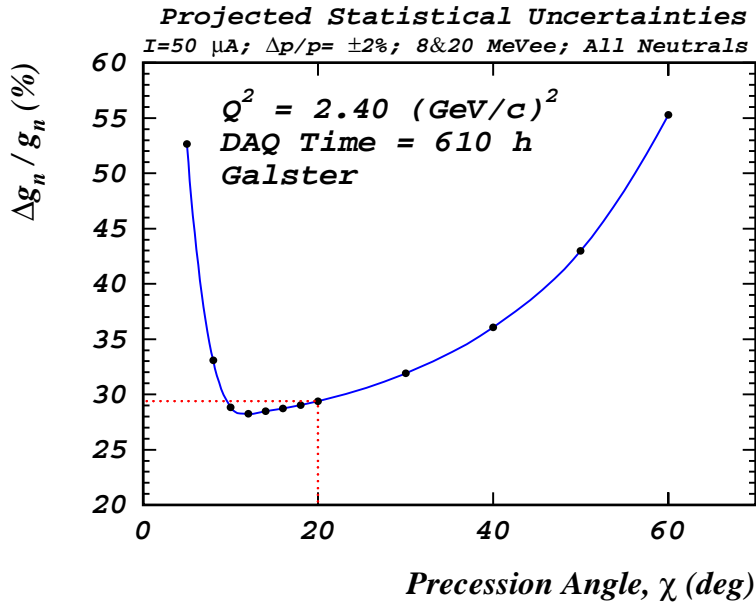


Figure 16: Statistical uncertainty, projected at  $Q^2 = 2.4 (\text{GeV}/c)^2$ , as a function of precession angle.

### 3.3 Count Rates

The rate of electron-neutron coincidence events, which comes from quasielastic scattering of electrons on the 15-cm LD<sub>2</sub> target, was projected for a beam current of 50  $\mu\text{A}$  (which corresponds to a beam luminosity  $L = 2.39 \times 10^{38} \text{ cm}^{-2}\text{s}^{-1}$ ). The calculation was done for a momentum bite  $\Delta p/p$  of  $\pm 2.0\%$  for the scattered electron. This restricted HMS momentum bite discriminates against neutrons associated with pion production and helps to suppress the “false asymmetry” neutrons from the two-step process  $d(\vec{e}, e' \vec{p})n + \text{Pb}(\vec{p}, \vec{n})$ . Protons that originate from quasielastic scattering at the angle of  $40.9^\circ$  will be deflected away from the front array of the polarimeter by the magnetic field of Charybdis. In exchange for these protons, the protons emitted from

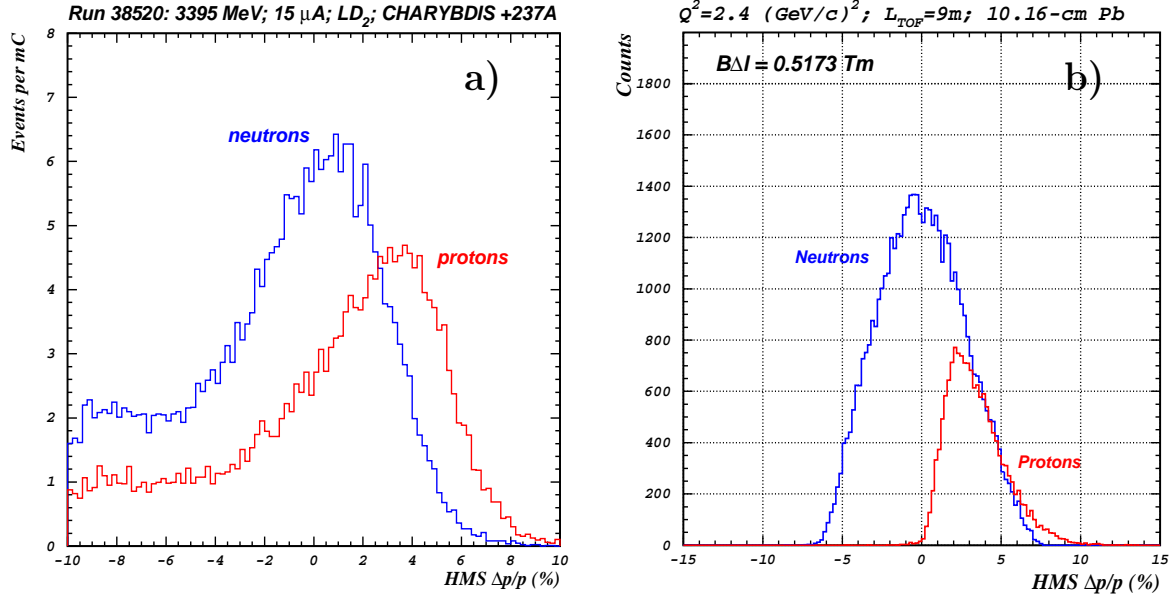


Figure 17: Momentum distributions for electrons in the HMS associated with neutrons and protons scattered into the polarimeter. Panel (a) shows spectra obtained in E93-038 at  $Q^2 = 1.47 \text{ (GeV/c)}^2$ . Panel (b) demonstrates a result of a simulation at  $Q^2 = 2.40 \text{ (GeV/c)}^2$ . The shift in the proton spectrum occurs because protons are deflected by the field of the Charybdis magnet. A cut on  $\Delta p/p$  ( $= \pm 2\%$ ) reduces the false asymmetry or asymmetry dilution from the two step process  $d(\vec{e}, e'\vec{p})n + Pb(\vec{p}, \vec{n})$  in the lead curtain ahead of the polarimeter.

the target at another angle (and corresponding to another value of  $Q^2$  and a “shifted” value of the momentum of the scattered electrons) will be deflected into the front array. This effect was observed in E93-038 (see Fig. 17), and application of a tight cut on the momentum of the electron in the HMS reduces this “false asymmetry” effect significantly. The restricted HMS momentum bite also helps to suppress the neutrons associated with pion production.

The acceptances for E93-038 were calculated for the HMS in the normal-quad mode and in the rear position. We used the kinematic conditions from Table 1 for the  $Q^2$  point of  $2.4 \text{ (GeV/c)}^2$ . Based on the acceptance-averaged coincidence rate  $\langle R_{\text{MCEEP}} \rangle$  from MCEEP [Ulmer (1991) version 3.1 includes radiative corrections], we estimated the real-event rate  $R_{\text{real}}$  for a neutron transmission  $t = 0.57$  [through a 10-cm Pb curtain], an HMS efficiency  $\epsilon_{\text{HMS}} = 0.92$  [which is the product of a single-hit fraction in the wire chambers (0.95) and an efficiency for tracking a good electron (0.97)], and a live-time fraction of the data-acquisition system of 0.95. We used a value of 0.0115 as an estimate of the neutron polarimeter efficiency value. This value is an extrapolation of the polarimeter efficiencies obtained in E93-038 for neutrons up to 786 MeV (see Fig. 12). Listed in Table 2 are neutron polarimeter and HMS acceptances, estimated neutron polarimeter parameters (viz.,  $A_Y$  and  $\epsilon_n$ ), and the calculated real event rate.

### 3.4 Projected Uncertainties

The up-down asymmetry, measured in E93-038, is proportional to the projection of the neutron polarization vector on the axis that is perpendicular to the neutron momentum direction. Thus,

HMS angular acceptance:	
$\Delta\theta_e$ (mrad)	$\pm 27.5$
$\Delta\phi_e$ (mrad)	$\pm 71.9$
Neutron polarimeter angular acceptance:	
$\Delta\theta_n$ (mrad)	$\pm 55.5$
$\Delta\phi_n$ (mrad)	$\pm 27.8$
Neutron polarimeter efficiency, $\epsilon_n$ (%)	1.15
MCEEP rate, $\langle R_{MCEEP} \rangle$ (Hz)	72.3
Real-event rate, $R_{real}$ (Hz)	0.44
Neutron polarimeter analyzing power, $A_Y$	0.085

Table 2: The neutron polarimeter and HMS acceptances, estimated neutron polarimeter parameters, and calculated real event rate at  $Q^2 = 2.4$  (GeV/c)<sup>2</sup>.

the ratio of asymmetries for neutron spin precession through  $\pm\chi$  degrees is given by:

$$\eta \equiv \frac{\xi_-}{\xi_+} = \frac{P_-^x}{P_+^x} = \frac{P_{S'} \cos(-\chi) + P_{L'} \sin(-\chi)}{P_{S'} \cos(\chi) + P_{L'} \sin(\chi)} = \frac{(P_{S'}/P_{L'}) \cos \chi - \sin \chi}{(P_{S'}/P_{L'}) \cos \chi + \sin \chi}, \quad (10)$$

yielding

$$(P_{S'}/P_{L'}) = -\frac{\sin \chi (\eta + 1)}{\cos \chi (\eta - 1)} = -\tan \chi \left( \frac{\eta + 1}{\eta - 1} \right). \quad (11)$$

Here  $P_{S'}$  and  $P_{L'}$  are transverse and longitudinal projections of the neutron polarization vector:

$$P_{S'} = -h P_e \frac{K_S g}{K_0 (1 + g^2/K_0)}, \quad (12)$$

and

$$P_{L'} = h P_e \frac{K_L}{K_0 (1 + g^2/K_0)}, \quad (13)$$

where  $h$  is the beam helicity,  $P_e$  is the beam polarization, and  $g \equiv (G_E/G_M)$ . Using

$$(P_{S'}/P_{L'}) = -g (K_S/K_L), \quad (14)$$

and Eq. (11) and Eq. (14) yields

$$g = -\left( \frac{K_L}{K_S} \right) \left( \frac{P_{S'}}{P_{L'}} \right) = \left( \frac{K_L}{K_S} \right) \tan \chi \left( \frac{\eta + 1}{\eta - 1} \right). \quad (15)$$

The statistical uncertainty in the  $g$  value is

$$(\delta g)_{stat} = \left( \frac{K_L}{K_S} \right) \tan \chi \frac{2}{(\eta - 1)^2} \delta \eta, \quad (16)$$

while the relative statistical uncertainty  $(\delta g/g)_{stat}$  is

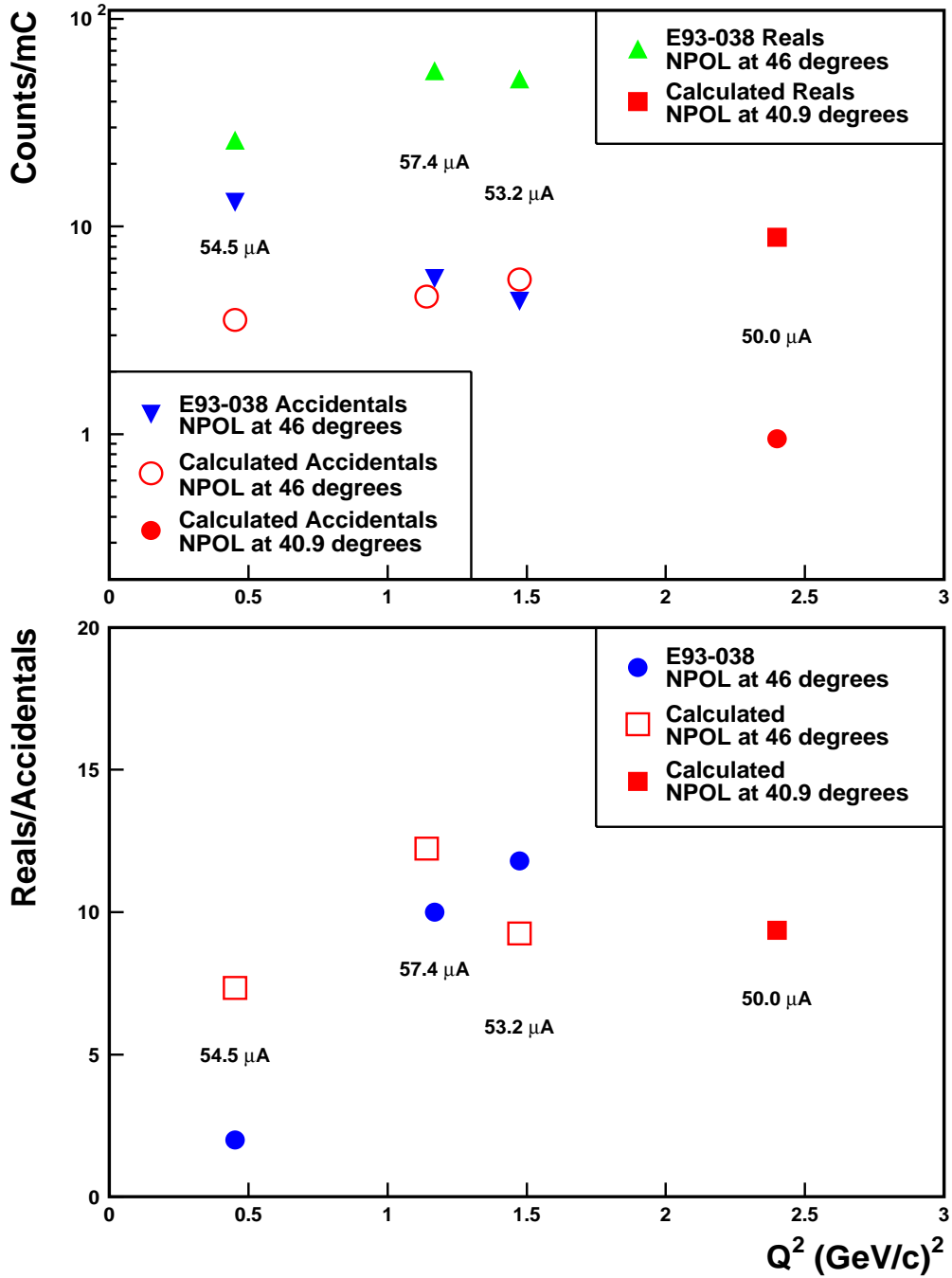


Figure 18: Real event rate, accidental coincidence rate, and the reals-to-accidentals ratio obtained from E93-038 and from a calculation at  $Q^2 = 2.4$   $(\text{GeV}/c)^2$ . The target-front array flight path was 7 m for NPOL at 46 degrees, and 9 m for NPOL at 40.9 degrees.

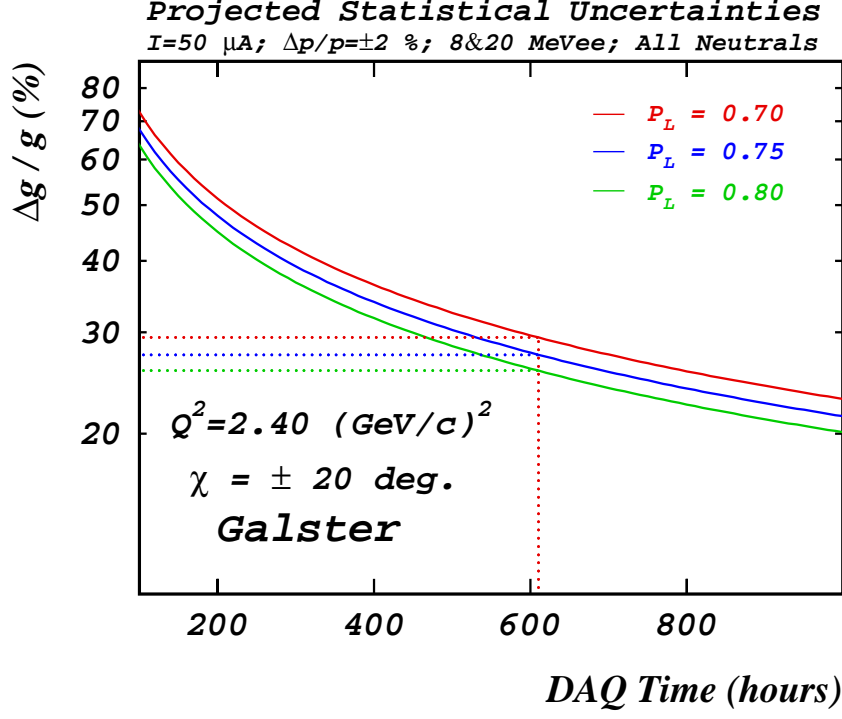


Figure 19: Projected uncertainty  $\Delta g_n/g_n$  as a function of the DAQ time. The beam current is  $50 \mu\text{A}$ , and the corrupted fraction (see text) is 25%.

$$\left(\frac{\delta g}{g}\right)_{stat} = \frac{2}{(\eta + 1)(\eta - 1)} \delta\eta. \tag{17}$$

Here  $\delta\eta$  is the statistical error in the asymmetry ratio

$$\left(\frac{\delta\eta}{\eta}\right)^2 = \left(\frac{\delta\xi_-}{\xi_-}\right)^2 + \left(\frac{\delta\xi_+}{\xi_+}\right)^2, \tag{18}$$

or

$$(\delta\eta)^2 = \left(\frac{\delta\xi_-}{\xi_+}\right)^2 + \xi_-^2 \left(\frac{\delta\xi_+}{\xi_+^2}\right)^2. \tag{19}$$

To project the statistical uncertainties, we used the statistical errors for asymmetries which come from Poisson statistics:

$$\left(\frac{\delta\xi_{\pm}}{\xi_{\pm}}\right)^2 = \frac{1}{\xi_{\pm}^2} \left(\frac{1 + 2/r}{N_{\pm}}\right) = \frac{1}{(A_Y P_{\pm}^x)^2} \left(\frac{1 + 2/r}{N_{\pm}}\right). \tag{20}$$

Here  $N_{\pm}$  is the number of events taken during  $\pm 20^\circ$  precession angle runs,  $A_Y$  is the polarimeter analyzing power, and  $r$  is the ratio of real-to-accidental coincidences. For these projections, the value  $r = 6$ . Values of  $r$  achieved in E93-038 are plotted in Fig. 18 as a function of  $Q^2$ . The accidental coincidence rates were calculated with a combination of the MONQEE code (Dytman

1987) for the electron single rates in the HMS and the program of P. Degtyarenko to calculate the neutron single rates in the polarimeter. This program, based on GEANT 3.21 (Brun 1993), uses the GCALOR (Zeitnitz 1994) program package in order to simulate hadronic interactions down to 1 MeV for nucleons and charged pions and into the thermal region for neutrons, and uses DINREG (Degtyarenko 1992, 2000) – Deep Inelastic Nuclear Reaction Exclusive Generator with a model for hadronic interactions of electrons and photons. The large difference between the measured and calculated accidentals and the ratios of real-to-accidental coincidences at  $Q^2 = 0.45 \text{ (GeV/c)}^2$  is because the calculation doesn't take into account the larger radiation background in the Hall C at this lowest beam energy of 884 MeV.

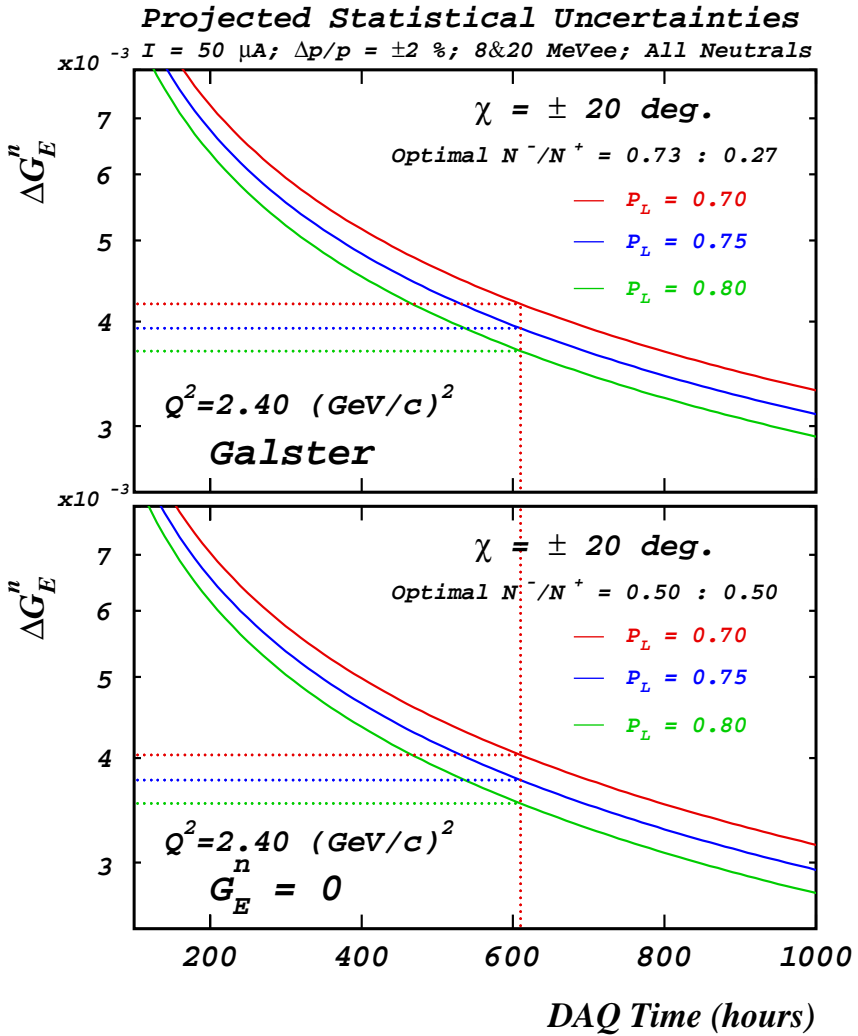


Figure 20: Projected uncertainty  $G_E^n$  as a function of the DAQ time for the Galster parameterization and  $G_E^n = 0$ . The beam current is  $50 \mu\text{A}$ , and the corrupted fraction is 25%.

The projected uncertainty  $\Delta g_n/g_n$  is plotted in Fig. 19 as a function of the data acquisition time for a luminosity of  $2.39 \times 10^{38} \text{ cm}^{-2}\text{s}^{-1}$ , which is achievable with a beam current of  $50 \mu\text{A}$  on a 15-cm liquid deuterium target. The DAQ time that is designated by the dotted line in Fig. 19 was chosen to target an uncertainty  $\Delta G_E^n$  in the vicinity of 0.004 [see Fig. 20 also], which

is comparable to the uncertainties obtained at  $Q^2 = 1.15$  and  $1.47$  (GeV/c)<sup>2</sup>. Because  $G_E^n$  is expected to be small and  $\Delta g/g$  is relatively large, the relative uncertainty in  $G_E^n$  is insensitive to the relative uncertainty in  $G_M^n$ . Projected statistical uncertainties in  $G_E^n$  with  $\Delta G_M^n/G_M^n = 0.050$  are plotted in Fig. 20 as a function of data acquisition time; the contribution of  $G_M^n$  to the uncertainty in  $G_E^n$  is small. Recent Hall B measurements of  $G_M^n$  up to  $Q^2 = 4.8$  (GeV/c)<sup>2</sup> [Brooks et al. (1994)], which are currently being analyzed, should reduce the relative uncertainties in  $G_M^n$ .

## 4 Some Results from E93-038

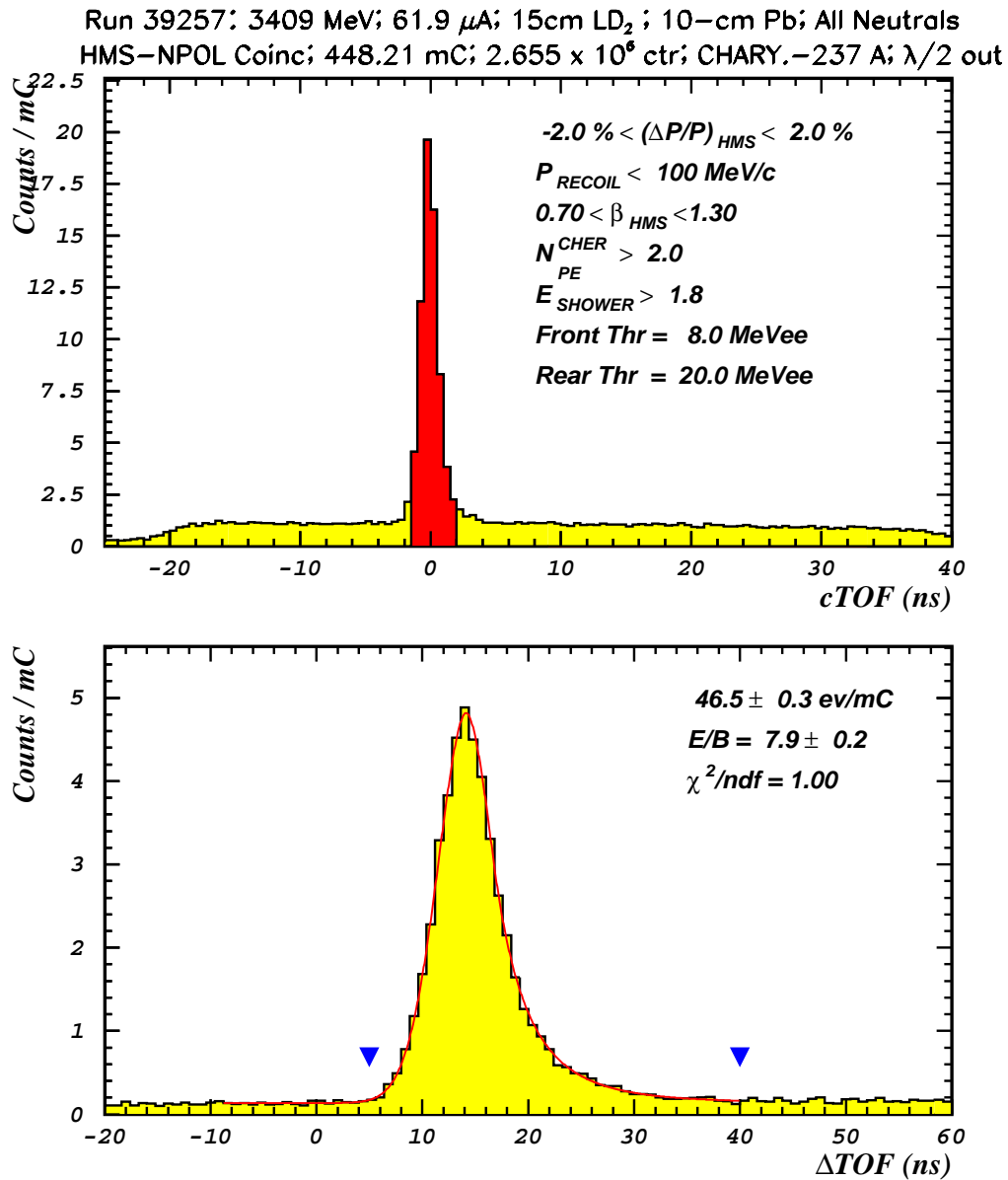
The purpose of this section is to indicate the quality of the data obtained in E93-038. The results shown here for the highest  $Q^2$  [viz.,  $Q^2 = 1.47$  (GeV/c)<sup>2</sup>] are based on an initial analysis of a limited sample of the runs. The top panel in Fig. 21 is an HMS-NPOL coincidence time-of-flight (cTOF) spectrum for all events generated by a neutron incident on the polarimeter. The incident neutron may scatter elastically to a detector in the rear array or it may cause a proton to be detected in the rear array. The designation “all neutrals” in the figures that follow refers to both (n,n) and (n,p) events. The FWHM of the cTOF spectrum is about 1.5 ns, and the reals-to-accidentals ratio is  $\approx 12$  at a beam current of  $\approx 50$   $\mu$ A [see Fig. 18]. The bottom panel in Fig. 21 is the time-of-flight spectrum between a neutron event in the front array of the polarimeter and an event in the rear array for both helicity states of the beam. It is called a  $\Delta$ TOF or dTOF spectrum. The dTOF spectrum can be subdivided into four spectra – two for each beam helicity state (L or R) with scattering to the upper (U) array or to the bottom (D) array; these four dTOF spectra (LU, LD, RU, and RD) appear in Fig. 22. The cross ratio and the asymmetry are calculated from these spectra. A preliminary analysis of the asymmetries for each run and the error-bar weighted average for these data appear in Fig. 23.

The correlation between cTOF and dTOF is shown in Fig. 24. This correlation at  $Q^2 = 1.14$  (GeV/c)<sup>2</sup> was obtained with the following cuts: (1) a mean-time window duration of 20 ns for both front and rear taggers, and (2) a radius of 30 cm around a neutron track must be free of a charged particle. Application of these cuts is possible only after time calibration procedures, as described by Kelly (2001a). Figure 25 illustrates the importance of time calibration also. This figure presents event rates measured in E93-038 at different beam currents. The deviation from plain proportionality between the event rate and the beam current is caused by corruption of electron-neutron coincidence events from accidental background particles (charged or neutral) that appear during the coincidence time window. The fraction of corrupted events (CF) at a certain beam current  $I$  can be calculated (see Fig. 27 ahead) from an estimate of the single rates in the HMS and the neutron polarimeter, and it can be expressed in terms of a measured blocking factor (BF):

$$CF(I) = \frac{BF(I) - 1}{BF(I)}, \quad (21)$$

where the blocking factor is

$$BF(I) = \frac{Rate(I)}{Rate(0)}. \quad (22)$$



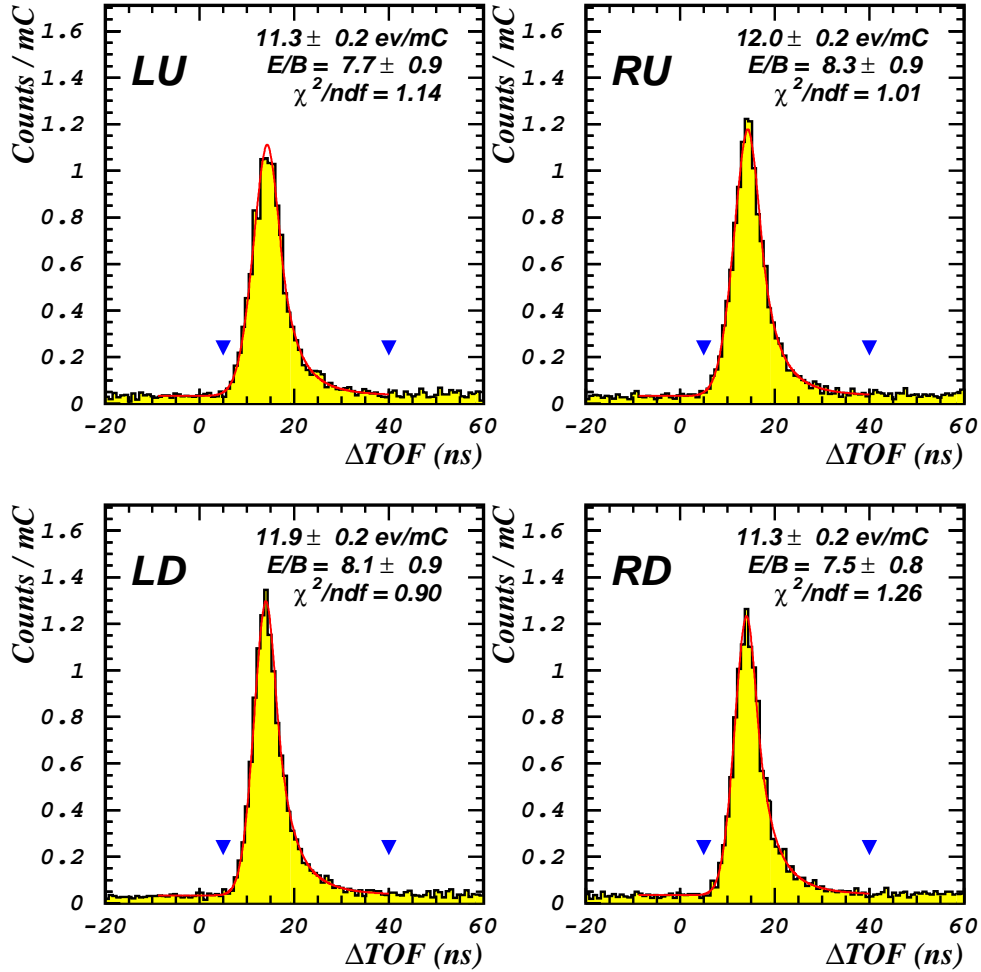
Run was started on Apr 11, 2001 at 20:48

Omitted Detectors : 22

Analysis (v2.1) done on 5/1/2001 by

Figure 21: cTOF (top panel) and dTOF (bottom panel) spectra for run 39257 at  $Q^2 = 1.47 \text{ (GeV}/c)^2$ .

Run 39257: 3409 MeV; 61.9  $\mu$ A; 15cm LD<sub>2</sub>; 10-cm Pb; All Neutrals  
 HMS-NPOL Coinc; 448.21 mC; 2.655 x 10<sup>6</sup> ctr; CHARY.-237 A;  $\lambda/2$  out



Beam (L/R) Asymmetry  $\xi_{LR} = -0.17 \pm 0.72 \%$

NPOL (U/D) Asymmetry  $\xi_{UD} = 0.00 \pm 0.72 \%$

Cross-Ratio  $r = 1.0577 \pm 0.0152$

Asymmetry  $\xi = 2.80 \pm 0.72 \%$

Analysis (v2.1) done on 5/ 1/2001 by

Figure 22: Four dTOF spectra (LU, LD, RU, and RD – see text) for run 39257 at  $Q^2 = 1.47$  (GeV/c)<sup>2</sup>.

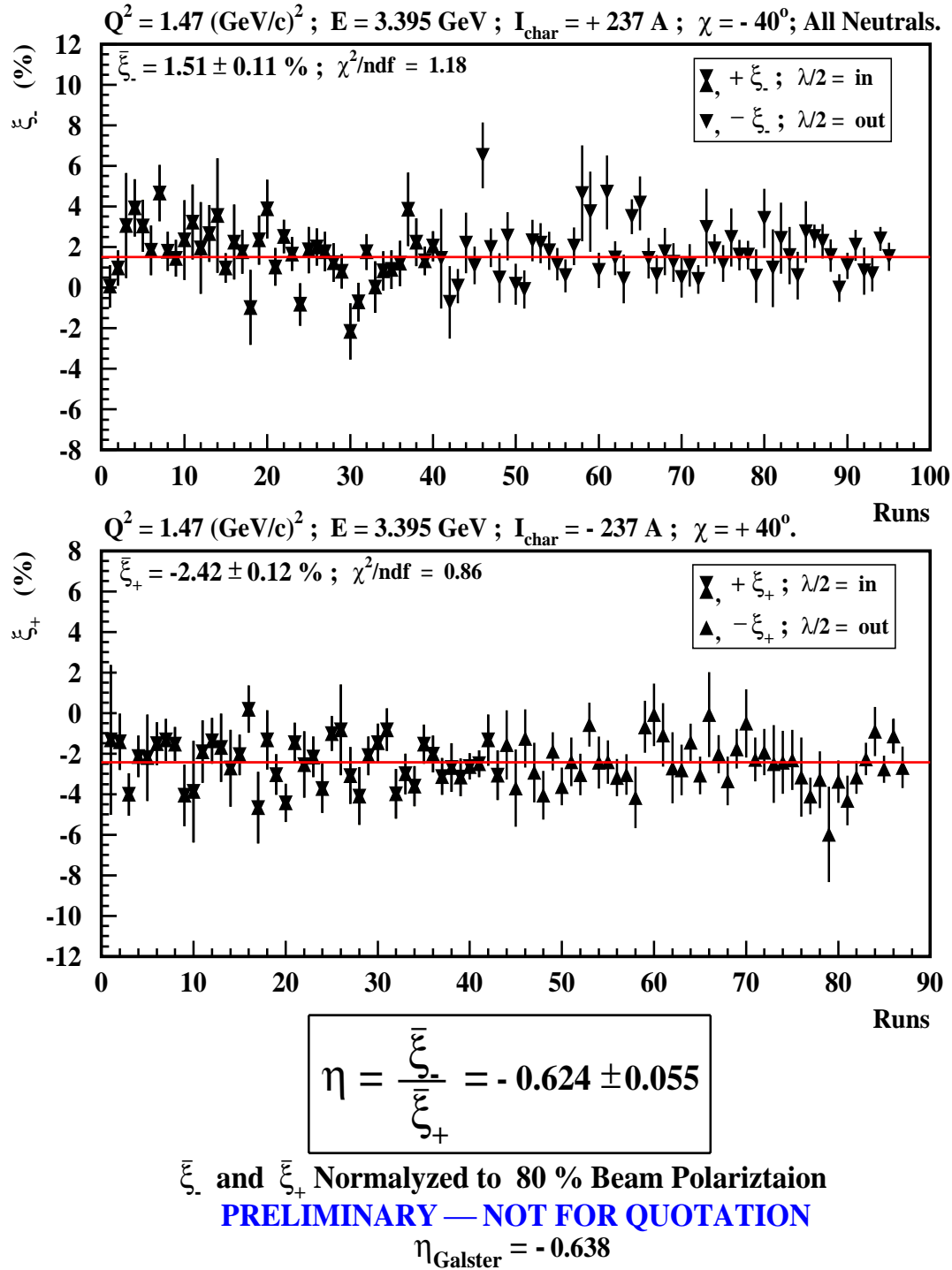


Figure 23: Asymmetries obtained from preliminary analysis of a data at  $Q^2 = 1.47 \text{ (GeV/c)}^2$  (not for quotation!).

Summary (4 Runs): 2329 MeV; Charybdis OFF; All Neutrals

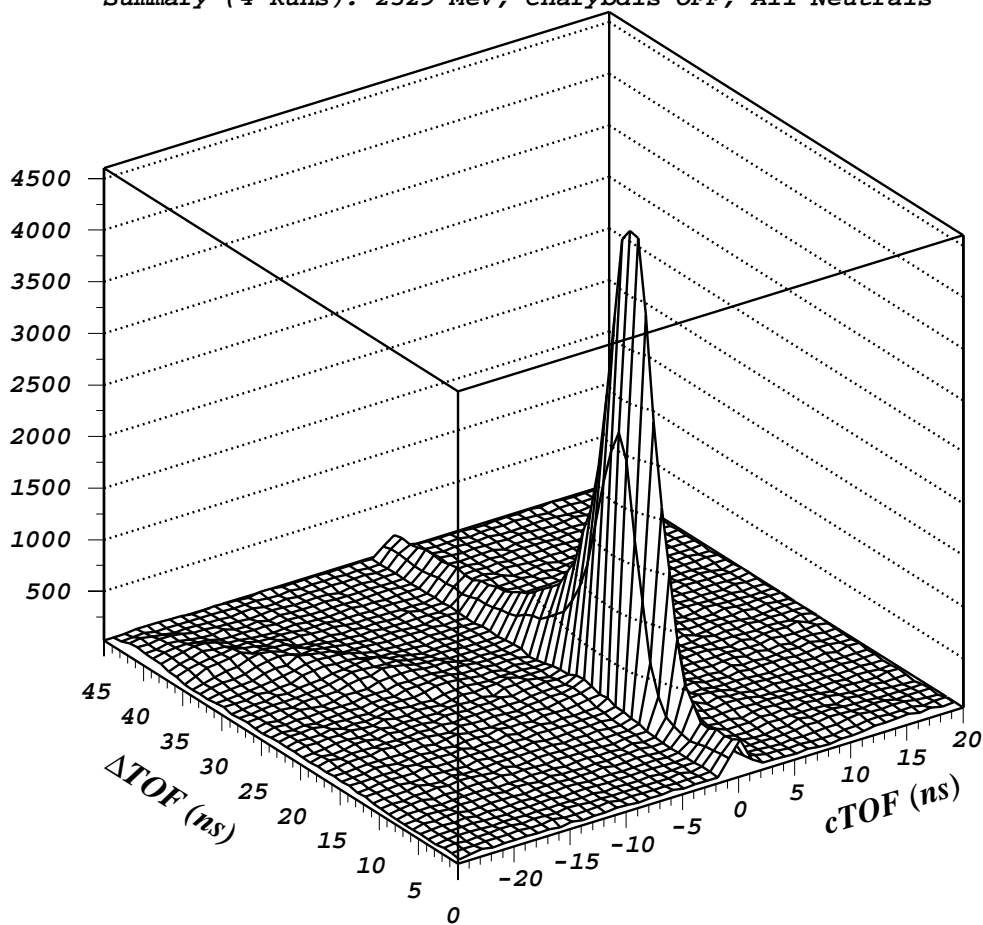
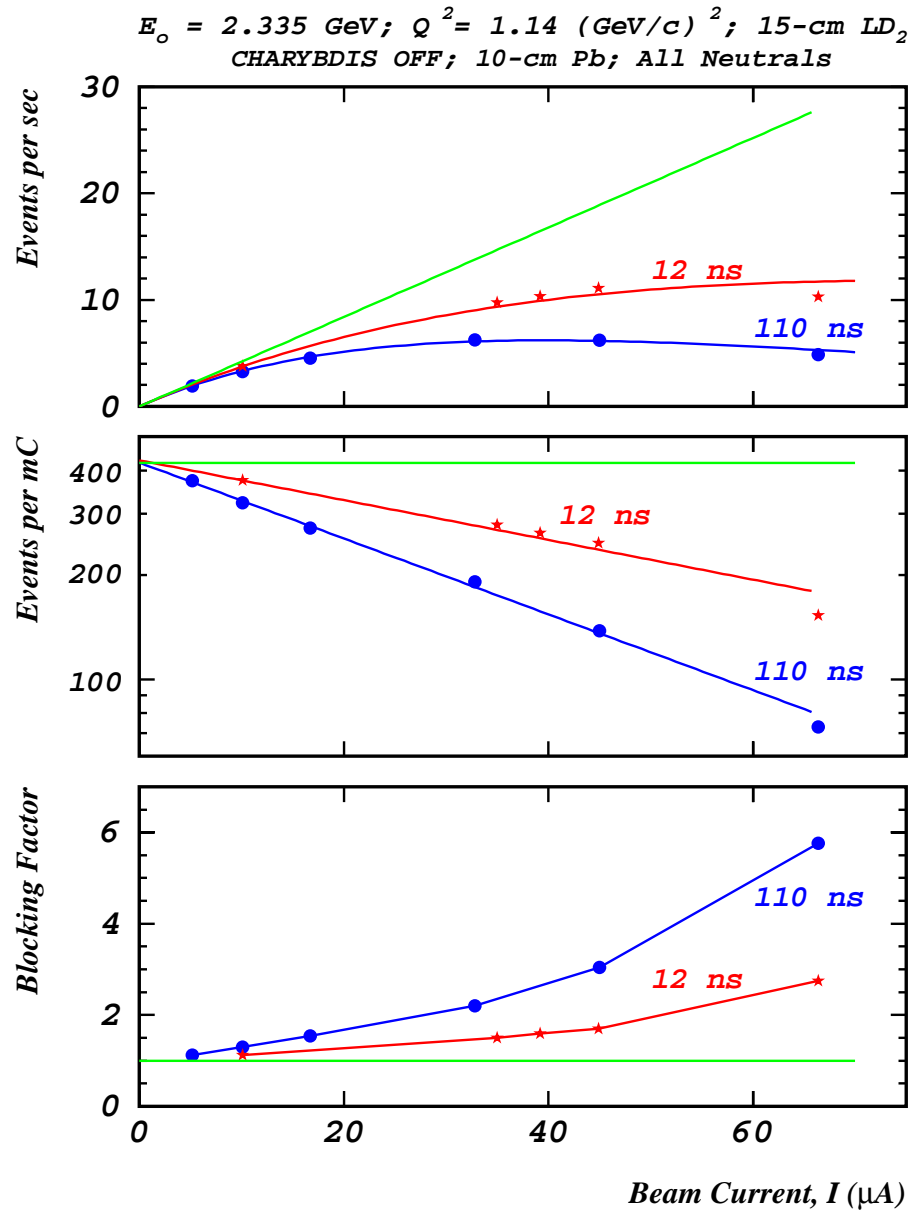


Figure 24: Correlation between cTOF and dTOF for summary of four runs at  $Q^2 = 1.14 \text{ (GeV}/c)^2$ .



12/14/2000

Figure 25: Event rate versus beam current at  $Q^2 = 1.14 \text{ (GeV/c)}^2$ .

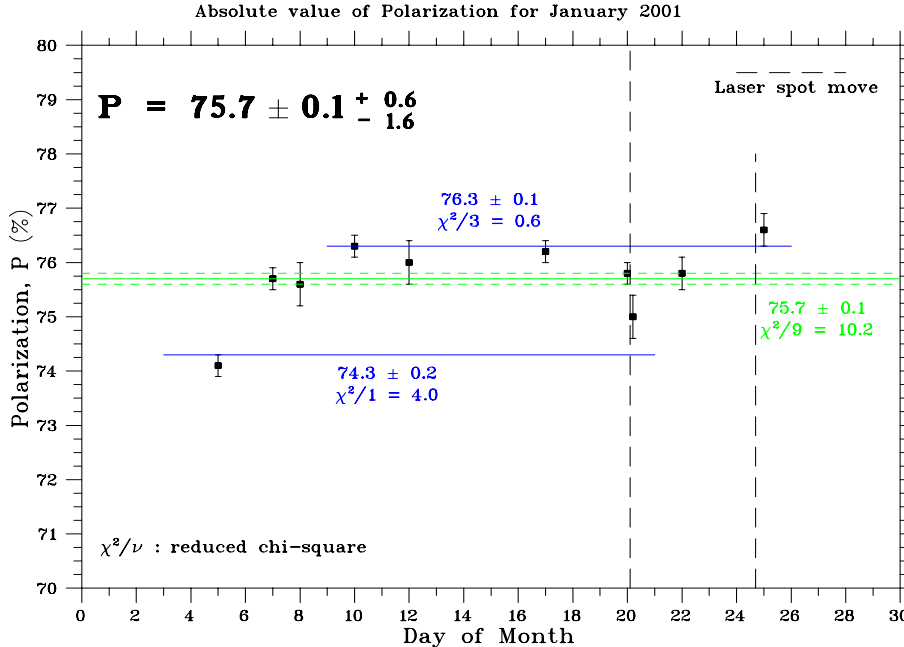


Figure 26: Electron beam polarization in January 2001.

Here  $Rate(I)$  is the number of events per mC of beam at beam current  $I$ , and  $Rate(0)$  is the approximation of this value for  $I = 0$ . As shown in Fig. 25, a tight (12 ns) “software” window makes a substantial reduction in the blocking factor (i.e., fraction of corrupted events).

The absolute values of the beam polarization measured in January 2001 are plotted in Fig. 26.

## 5 Beam Time

We estimate that 610 hours of acquisition time for “good” runs on a 15-cm LD<sub>2</sub> target will be needed to produce a statistical uncertainty  $\Delta G_E^n$  in the vicinity of 0.004 at  $Q^2 = 2.40$  (GeV/c)<sup>2</sup>. These 610 hours will require a beam polarization of 70% at a current of 50  $\mu$ A on a 15-cm LD<sub>2</sub> target. The projection was based on a calculation of a fraction of electron-neutron coincidence events corrupted from a background particle (charged or neutral) that appears during the coincidence time window. For a 50  $\mu$ A beam, the corrupted fraction is calculated to be 25% (see Fig. 27). We estimate that 96 hours of acquisition time for runs on a 15-cm LH<sub>2</sub> target will be needed to assess the false asymmetry or dilution from the two-step process  ${}^2\text{H}(\vec{e}, e'\vec{p})\text{n} + \text{Pb}(\vec{p}, \vec{n})$ .

Our beam-time request for measuring  $G_E^n$  at  $Q^2 = 2.40$  (GeV/c)<sup>2</sup> is shown in Table 3.

*The proposed measurements can be done also in Hall A. It turns out that the counting rates are essentially the same. This collaboration is willing to run in Hall A if the experiment can be scheduled earlier in Hall A than in Hall C.*

## 6 Collaboration

Each of the participants listed earlier contributed to the success of E93-038. The collaboration is a strong, experienced, and large team (currently about 70 scientists from 22 institutions).

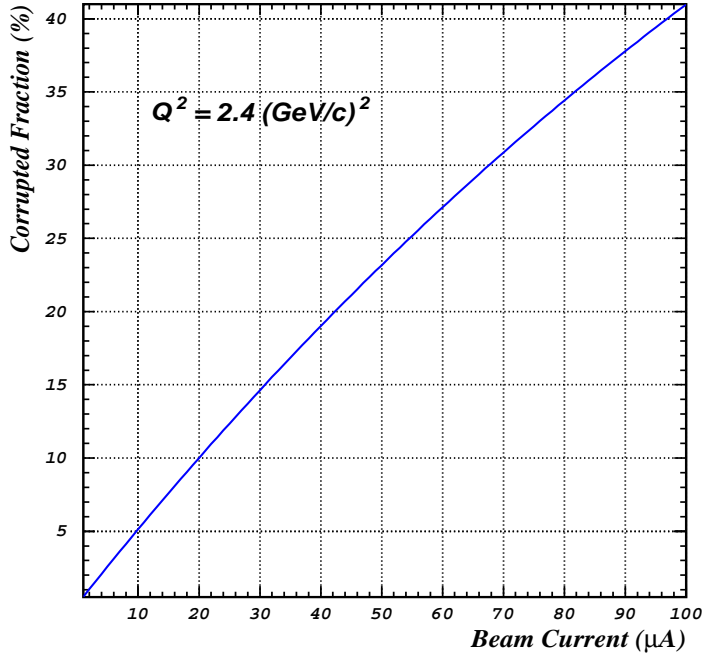


Figure 27: Calculated fraction of electron-neutron coincidence events corrupted from a background particle (charged or neutral) that appears during the coincidence time window of 70 ns as a function of the beam current.

Graduate students will be added after the proposed experiment is approved and scheduled.

As in E93-038, Kent State University (KSU) will be responsible for the neutron polarimeter; MIT, for CHARYBDIS; and JLab for the HMS. KSU provided the neutron detectors in the rear array and the polarimeter electronics; Hampton University provided one-half of the neutron detectors in the front array, while JLab provided the other half. The University of Virginia provided the tagger detectors used in E93-038. Duke University took responsibility for the Analysis Engine and also for setting up the electronics and timing. Professor James J. Kelly at the University of Maryland spearheaded the development of the analysis programs used in E93-038, and Dr. A.Yu. Semenov is the czar of the E93-038 analysis effort. T. Reichelt (Bonn), H. Fenker (JLab), and S. Danagoulian (NCAT) were the lead scientists in establishing the operating conditions for running the Moeller polarimeter at a beam energy below one GeV, and in setting up and running the Moeller polarimeter at the two higher energies. A. Ahmidouch (NCAT) and S. Taylor (MIT) were the lead scientists in mapping the CHARYBDIS dipole magnet. A. Ahmidouch (NCAT) was the lead scientist in preparing the run plan to obtain data for new matrix elements for the HMS. For this proposal, the personnel at the same institutions will provide their expertise. With respect to equipment, we anticipate the need for a few additional 10-in  $\times$  40-in  $\times$  4-in neutron detectors in order to replace the 20-in  $\times$  40-in  $\times$  4-in detectors in the rear array. Kent State University did not have quite enough to replace each 20-in  $\times$  40-in  $\times$  4-in detector with two 10-in  $\times$  40-in  $\times$  4-in detectors in E93-038.

	Hours	Days
Commissioning without beam		
Pulse-height calibration and cosmic-ray tests	168	7
Commissioning with beam		
HMS	24	1
Moeller Polarimeter	24	1
NPOL (check detectors, adjust timing, adjust thresholds, adjust Pb curtain thickness, determine optimal beam current, shadow shield, etc.)	62	2.6
Total commissioning with beam	<b>110</b>	<b>4.6</b>
$G_E^n$ physics measurements		
LD <sub>2</sub> target	610	25.4
LH <sub>2</sub> target	96	4
Dummy target	72	3
Beam polarization	72	3
Time calibrations [LD <sub>2</sub> target]	48	2
Overhead <sup>(a)</sup>	72	3
Total $G_E^n$ physics measurements	<b>970</b>	<b>40.4</b>
Total beam time for $G_E^n$ at $Q^2 = 2.40$ (GeV/c) <sup>2</sup>	<b>1080</b>	<b>45</b>

Table 3: Beam-time request for measuring  $G_E^n$  at  $Q^2 = 2.40$  (GeV/c)<sup>2</sup> for a 50  $\mu$ A, 70% polarized beam on a 15-cm LD<sub>2</sub> target.

---

(a) 144 changes in Charybdis dipole current, 72 target changes, starting and stopping the DAQ system at least 850 times for runs that are typically 2 hours long.

## References

- [Arenhoevel 1987] H. Arenhoevel, Phys. Lett. **B199**, 13 (1987).
- [Arenhoevel 1988] H. Arenhoevel *et al.*, Z. Phys. **A331**, 123 (1988).
- [Arndt 1977] R.A. Arndt, R.H. Hackman, and L.D. Roper, Phys. Rev. **C15** 1002 (1977).
- [Arndt 2000] R. A. Arndt, L. D. Roper *et al.*, Scattering Analysis Interactive Dial-In (SAID) Program. Virginia Polytechnic Institute and State University, Unpublished. The Virginia Tech Partial-Wave Analysis Facility is still available from the original web site <http://said.phys.vt.edu/>. This facility is available on-line at <http://www.gwdac.phys.gwu.edu/> from the CNS Data Analysis Center at The George Washington University.

- [Aznaurian 1993] I.G. Aznaurian, Phys. Lett. **B316**, 391 (1993).
- [Beck 1992] G. Beck and H. Arenhoevel, Few Body Systems **13**, 165 (1992).
- [Brun 1993] R. Brun et al. *GEANT Detector Description and Simulation Tool*. CERN Program Library Long Writeup W5013, September 1993.
- [Cardarelli 2000] F. Cardarelli, S. Simula, Phys. Rev. **C62**, 065201 (2000).
- [Cecil 1979] R. Cecil, B.D. Anderson, R. Madey. Nucl. Instrum. Meth. **161**, 439 (1979).
- [Chung 1991] P.L. Chung and F. Coester, Phys. Rev. **D44**, 229 (1991).
- [Degtyarenko 1992] P.V. Degtyarenko, M.V. Kossov. *Monte Carlo Program for Nuclear Fragmentation*. Preprint ITEP 11-92, Moscow (1992).
- [Degtyarenko 2000] P.V. Degtyarenko, M.V. Kossov, and H.-P. Wellisch. *Chiral invariant phase space event generator*. Eur. Phys. J. A **8**, 217-222 (2000); A **9**, 411-420 (2000); A **9**, 421-424 (2000).
- [Dong 1998] S.J. Dong, K.F. Liu, and A.G. Williams, Phys. Rev. **D58**, 074504 (1998).
- [Drechsel 1989] D. Drechsel and M.M. Giannini, Rep. Prog. Phys. **52**, 1083 (1989).
- [Dytman 1987] S. Dytman. Private Communication (1987).
- [Eden 1994] T. Eden *et al.*, Phys. Rev. **C50**, R1749 (1994).
- [Feshbach 1967] H. Feshbach and E. Lomon, Rev. Mod. Phys. **39**, 611 (1967).
- [Frank 1996] M.R. Frank, B.K. Jennings, and G.A. Miller, Phys. Rev. **C54**, 920 (1996).
- [Friar 1990] J.L. Friar, Phys. Rev. **C42**, 2310 (1990).
- [Gari 1985] M.F. Gari and W. Krumpelmann, Z. Phys. **A322**, 689 (1985).
- [Gari 1992] M.F. Gari and W. Krumpelmann, Phys. Lett. **B274**, 159 (1992).
- [Galster 1971] S. Galster, H. Klein, J. Moritz, K.H. Schmidt, D. Wegener, and J. Blechwenn, Nucl. Phys. **B32**, 221 (1971).
- [Herberg 1999] C. Herberg *et al.*, Eur. Phys. J. **A5**, 131 (1999).
- [Holzwarth 1996] G. Holzwarth, Z. Phys. **A356**, 339 (1996).
- [Isgur 1998] N. Isgur, Phys. Rev. Lett. **83**, 272 (1999).
- [Isgur 2000] N. Isgur and J.W. Negele, Nuclear Theory with Lattice QCD, a proposal to DOE, PI's (2000).
- [Ji 1991] X. Ji, Phys. Lett. **B254**, 456 (1991).

- [Jones 2000] M. Jones *et al.*, Phys. Rev. Lett. **84**, 1398 (2000).
- [Kelly 2001a] J.J. Kelly, Time Calibration Procedures for E93-038 Polarimeter: Version 2.2, JLab E93-038 internal report (2001),  
URL: [http://www.physics.umd.edu/enp/e93038/time\\_calibration.ps](http://www.physics.umd.edu/enp/e93038/time_calibration.ps)
- [Kelly 2001b] J.J. Kelly, hep-ph/0111251, submitted to Phys. Rev. Lett. (unpublished).
- [Klein 1997a] F. Klein and H. Schmieden, Nucl. Phys. **A623**, 323c (1997).
- [Klein 1997b] F. Klein, Proc. of the 14th Int. Conf. on Particles and Nuclei, ed. by C.E. Carlson and J.J. Domingo, World Scientific 1997, p.121.
- [Kroll 1992] P. Kroll, M. Schurmann, and W. Schweiger, Z. Phys. **A342**, 429 (1992).
- [Laget 1990] J.M. Laget, Phys. Lett. **B273**, 367 (1990).
- [Liu 2001] K.F. Liu, Private Communication (2001).
- [Lu 1998] D.H. Lu, A.W. Thomas, and A.G. Williams, Phys. Rev. **C57**, 2628 (1998).
- [Lung 1993] A. Lung *et al.*, Phys. Rev. Lett. **70**, 718 (1993).
- [Madey 1995] R. Madey, A. Lai, and T. Eden, Polarization Phenomena in Nuclear Physics, edited by E.J. Stephenson S.E. Vigelor, AIP Proceedings No. 339, 47-54 (1995).
- [Mergell 1996] P. Mergell, U.G. Meissner, D. Drechsel, Nucl. Phys. **A596**, 367 (1996).
- [Meyerhoff 1994] M. Meyerhoff *et al.*, Phys. Lett. **B327**, 201 (1994).
- [Mosconi 1991] B. Mosconi, J. Pauchenwein, and P. Ricci, Proceedings of the XIII European Conference on Few-Body Problems in Physics, Marciana Marina (Elba), Italy (September 1991).
- [Ohlsen 1973] G.G. Ohlsen and P.W. Keaton, Jr., Nucl. Instr. Meth. **109**, 41 (1973).
- [Ostrick 1994] M. Ostrick *et al.*, Phys. Rev. Lett. **83**, 276 (1999).
- [Pace 2000] E. Pace, G. Salme, F. Cardarelli, and S. Simula, Nucl. Phys. **A666**, 33 (2000).
- [Passchier 1999] I. Passchier *et al.*, Phys. Rev. Lett. **82**, 4988 (1999).
- [Platchkov 1990] S. Platchkov *et al.*, Nucl. Phys. **A508**, 343c (1990).
- [Radyushkin 1984] A.V. Radyushkin, Acta Phys. Polon. **B15**, 403 (1984).
- [Rekalo 1989] M.P. Rekalo, G.I. Gakh, and A.P. Rekalo, J. Phys. **G15**, 1223 (1989).
- [Rohe 1999] D. Rohe *et al.*, Phys. Rev. Lett. **83**, 4257 (1999).
- [De Sanctis 2000] M. De Sanctis, M.M. Giannini, L. Repetto, and E. Santopinto, Phys. Rev. **C62**, 025208 (2000).

- [Schiavilla 2001] R. Schiavilla and I. Sick, Phys. Rev. **C64**, 041002 (2001).
- [Schmieden 1996] H. Schmieden, Proc. of the 12th Int. Symposium on High-Energy Spin Physics, Amsterdam (1996), ed. by C.W. de Jager et al., World Scientific 1997, p.538.
- [Ulmer 1991] P.E. Ulmer, MCEEP – Monte Carlo for Electro-Nuclear Coincidence Experiments, CEBAF–TN–91–101 (1991).
- [Zeitnitz 1994] C. Zeitnitz and T.A. Gabriel, Nucl. Instrum. Meth. **A349**, 106 (1994).
- [Zhu 2001] H. Zhu *et al.*, Phys. Rev. Lett. **87**, 081801 (2001).

# Appendix A

## Nucleon Charge and Magnetization Densities

James J. Kelly

*Department of Physics, University of Maryland, College Park, MD 20742*

(November 20, 2001)

A Fourier-Bessel analysis is used to fit charge and magnetization densities to data for the nucleon Sachs form factors. The neutron and proton magnetization densities are very similar, but the proton charge density is significantly softer. A useful measurement of the neutron charge density is obtained, although the relative uncertainty in the interior will remain substantially larger than for the other densities until precise new data at higher  $Q^2$  become available.

The Sachs form factors  $G_E$  and  $G_M$  are determined by the charge and magnetization distributions within nucleons and have been measured by numerous experiments on elastic electron scattering from the proton or quasielastic scattering from the neutron in deuterium or polarized  $^3\text{He}$ . Early experiments with modest  $Q^2$  suggested that

$$G_{Ep} \approx \frac{G_{Mp}}{\mu_p} \approx \frac{G_{Mn}}{\mu_n} \approx G_D$$

where  $G_D(Q^2) = (1 + Q^2/\Lambda^2)^{-2}$  with  $\Lambda^2 = 0.71$   $(\text{GeV}/c)^2$  is known as the dipole form factor. Data for  $G_{Mp}$  and  $G_{Mn}$  with  $Q^2 > 1$   $(\text{GeV}/c)^2$  show significant departures from the simple dipole parametrization, but the extraction of  $G_{Ep}$  from cross section data becomes increasingly difficult as  $Q^2$  increases. Recent data using the recoil polarization technique [1,2] have shown a dramatic, almost linear, decrease in  $G_{Ep}/G_{Mp}$  for  $Q^2 > 1$   $(\text{GeV}/c)^2$ . It was suggested that those results demonstrate that the proton charge is distributed over a larger volume than its magnetization, but radial densities were not obtained. In this paper we use a Fourier-Bessel analysis, together with a relativistic relationship between form factors and densities, to determine the nucleon charge and magnetization densities.

Let  $\rho_{ch}(r)$  and  $\rho_m(r)$  represent spherical intrinsic charge and magnetization densities. The vector magnetization density is then expressed as  $\vec{\mu}(r) = \mu\rho_m(r)\vec{\sigma}$  where  $\mu$  is the magnetic moment and  $\vec{\sigma}$  is the Pauli spin vector. It is convenient to normalize these densities according to

$$\int dr r^2 \rho_{ch} = Z \quad (1a)$$

$$\int dr r^2 \rho_m = 1 \quad (1b)$$

where  $Z = 0, 1$  is the nucleon charge. Fourier-Bessel transforms of the intrinsic densities are defined by

$$\tilde{\rho}(k^2) = \int dr r^2 j_0(kr)\rho(r) \quad (2)$$

where  $k^2$  is the square of the spatial frequency (or wave number).

The interpretation of the Sachs form factors appears simplest in the Breit frame for which the energy transfer vanishes. In this frame the nucleon approaches with initial momentum  $-\vec{q}_B/2$ , receives three-momentum transfer  $q_B$ , and leaves with final momentum  $\vec{q}_B/2$ . The Breit frame momentum is given by  $q_B^2 = Q^2 = q^2/(1 + \tau)$  where  $(\omega, \vec{q})$  is the momentum transfer in the laboratory,  $Q^2 = q^2 - \omega^2$  is the spacelike invariant four-momentum transfer,  $\tau = Q^2/4m^2$ , and  $m$  is the nucleon mass. The Sachs form factors are then determined by charge and magnetization transition form factors between states with opposite momentum

$$G_E(q_B^2) = \tilde{\rho}_{B,ch}(q_B^2) \quad (3a)$$

$$G_M(q_B^2) = \mu\tilde{\rho}_{B,m}(q_B^2) \quad (3b)$$

that resemble Fourier transforms of spatial densities. However, there exists no rigorous model-independent relationship between these transition form factors and the static charge and magnetization densities in the nucleon ground state with identical initial and final states. It is difficult to construct such a relationship because the boost operator for a composite system depends upon the interactions among its constituents. The first attempt to relate elastic form factors to ground-state densities was made by Licht and Pagnamenta [3] using a cluster model and a kinematic boost that neglects interactions. The transition form factors were then evaluated using the impulse approximation and neglecting relative motion. Ji [4] made a more rigorous analysis using a relativistic Skyrminion model based upon a Lorentz invariant Lagrangian density for which the classical soliton solution can be evaluated in any frame. Quantum fluctuations were then evaluated after the boost. Although an approximation is still required to evaluate the transition form factors, it was argued that this approximation is best in the Breit frame. The final results offer simple relationships between Sachs form factors and static densities that take the form

$$\tilde{\rho}_{ch}(k^2) = G_E(Q^2) \quad (4a)$$

$$\tilde{\rho}_m(k^2) = G_M(Q^2)(1 + \tau) \quad (4b)$$

where the internal spatial frequency  $k$  is related to the invariant momentum transfer by

$$k^2 = \frac{Q^2}{1 + \tau} \quad (5)$$

The most important relativistic effect is the Lorentz contraction of spatial distributions in the Breit frame and the corresponding increase of spatial frequency represented by the factor of  $(1 + \tau)$  in Eq. (5). A measurement with Breit-frame momentum transfer  $q_B = Q$  probes a reduced spatial frequency  $k$  in the rest frame. The Sachs form factor for a large invariant momentum transfer  $Q^2$  is determined by a much smaller spatial frequency  $k^2 = Q^2/(1 + \tau)$  and thus declines much less rapidly with respect to  $Q^2$  than the Fourier transform of the density declines with respect to  $k^2$ . In fact, the accessible spatial frequency is limited to  $k \leq 2m$  such that the Sachs form factors for large  $Q^2$  are determined by the Fourier transform of intrinsic densities in the immediate vicinity of the limiting frequency  $k_m = 2m$ , which is related to the nucleon Compton wavelength. The difference between the multiplicative factors for  $\rho_{ch}$  and  $\rho_m$  arises from the Lorentz transformation properties of scalar and vector fields [4]. Hence, the corresponding densities would differ even if the Sachs form factors were identical.

To extract radial densities from the nucleon form factor data we employ techniques originally developed for fitting radial distributions to data for scattering of electrons or protons from nuclei [5–7]. Simple models with a small number of parameters do not offer sufficient flexibility to provide a realistic estimate of the uncertainty in a radial density. Rather, we employ linear expansions in complete sets of basis functions that are capable of describing any plausible radial distribution without strong *a priori* constraints upon its shape. Such expansions permit one to estimate the uncertainties in the fitted density due to both the statistical quality of the data and the inevitable limitation of experimental data to a frequency range,  $k \leq k_{max}$ . The uncertainty due to limitation of  $k$  is known as *incompleteness error*. More detailed discussion of the method may be found in Refs. [5–7], but the basic idea is to supplement the experimental data by pseudodata of the form  $\tilde{\rho}(k_i^2) = 0 \pm \delta\tilde{\rho}(k_i^2)$  whose uncertainties are based upon a reasonable model of the asymptotic behavior of the form factor for  $k_i > k_{max}$  where  $k_{max}$  is the spatial frequency corresponding to the maximum measured  $Q^2$ . On quite general grounds one expects the asymptotic form factor for a confined system to decrease more rapidly than  $k^{-4}$  [6]. Therefore, we assume that

$$\delta\tilde{\rho}(k^2) = \tilde{\rho}(k_{max}^2) \left( \frac{k_{max}}{k} \right)^4 \quad (6)$$

The Fourier-Bessel expansion (FBE) takes the form

$$\rho(r) = \sum_n a_n j_0(k_n r) \Theta(R - r) \quad (7)$$

where  $\Theta$  is the unit step function,  $R$  is the expansion radius,  $k_n = n\pi/R$  are the roots of the Bessel function, and  $a_n$  are the coefficients to be fitted to data. One advantage of the FBE is that the contribution of each term to the form factor is concentrated around its  $k_n$  so that a coefficient  $a_n$  is largely determined by data with  $k \sim k_n$ . The larger the expansion radius  $R$ , the smaller the spacing between successive  $k_n$  and the greater the sensitivity one has to variations in the form factor. One should choose  $R$  to be several times the root-mean-square radius but not so large that an excessive number of terms is needed to span the experimental range of momentum transfer. Terms with  $k_n > k_{max}$  provide an estimate of the incompleteness error. We chose  $R = 4.0$  fm, but the results are insensitive to its exact value. Small but undesirable oscillations in fitted densities at large radius were suppressed using a *tail bias* based upon the method discussed in Ref. [8]. We employed a tail function of the form  $t(r) \propto e^{-\Lambda r}$ , based upon the successful dipole parametrization for low  $Q^2$ , and included in the  $\chi^2$  fit a penalty for strong deviations from the tail function for  $r > 2.0$  fm. The constraint on the neutron charge was also enforced using a penalty function. The tail bias improves the convergence of moments of the density but has practically no effect upon a fitted density in the region where it is large. The error band for a fitted density is computed from the covariance matrix for the  $\chi^2$  fit and includes the incompleteness error.

We selected the best available data in each range of  $Q^2$ , with an emphasis upon recent data using recoil or target polarization wherever available.  $G_{Mp}$  data were taken from the compilation of Höhler [9] for  $Q^2 < 0.15$  (GeV/c)<sup>2</sup> and for larger  $Q^2$  from the analysis of Brash *et al.* [10] using the recent recoil polarization data for  $G_{Ep}/G_{Mp}$  from Refs. [1,2]. Cross section data from Refs. [11,12] were used for  $Q^2 < 1$  (GeV/c)<sup>2</sup> but cross section data for  $G_{Ep}$  were excluded for larger  $Q^2$ . Similarly, the data for  $G_{En}$  were limited to recent polarization data [13–18], including the analysis of  $t_{20}$  and  $T_{20}$  by Schiavilla and Sick [19], and the neutron charge radius from Ref. [20]. Finally, for  $G_{Mn}$  we selected polarization data from [21] and cross section data from [22–28].

Fits to the form factor data are shown in Fig. 1 as bands that represent the uncertainties in the fitted form factors. The relative uncertainties become quite large for  $Q^2$  beyond the range of the experimental data but, with the exception of the neutron charge density, the impact of those uncertainties upon the fitted densities is slight because the form factors have become rather small by then. Although the low- $Q^2$  data for  $G_{Mn}$  have improved in recent years, significant systematic discrepancies remain. Recent data from Refs. [21,25,27,28] with small statistical uncertainties suggest a small dip near 0.2 and

a peak near 1 (GeV/c)<sup>2</sup>. For  $G_{En}$  we plot the Galster model [29] for comparison. The simple two-parameter fit Galster *et al.* made to the rather poor data available at that time did not permit a realistic estimate of the uncertainty in the form factor or fitted density and the apparent agreement with more modern data must be judged as remarkable but fortuitous.

Proton charge and magnetization densities are compared in Fig. 2. Both densities are measured very precisely, with interior uncertainties better than 1%. The new recoil-polarization data for  $G_{Ep}$  decrease more rapidly than either the dipole form factor or the magnetic form factor for  $Q^2 > 1$  (GeV/c)<sup>2</sup>; consequently, the charge density is significantly softer than the magnetization density of the proton. Neutron densities are shown in Fig. 3. We find that the magnetization density for the neutron is very similar to that for the proton, although the interior precision is not as good because the range of  $Q^2$  is smaller and the experimental uncertainties larger. Limitations in the range and quality of the  $G_{En}$  data presently available result in a substantially wider error band for the neutron charge density. Data at higher  $Q^2$  are needed to improve the interior precision, but a useful measurement of the interior charge density is obtained nonetheless. The positive interior density is balanced by a negative surface lobe. Note that polarization measurements are sensitive to the sign of the density, but that cross section measurements are not.

Having established that it is possible to fit physically reasonable charge and magnetization densities to elastic form factor data spanning a large range of  $Q^2$ , it is necessary to return to the question of the uniqueness of Eq. (4). The most important relativistic feature of that relationship is the identification of the spatial frequency  $k^2$  with  $Q^2/(1 + \tau)$  due to Lorentz contraction of distributions in the Breit frame and is common to most models. The relationships obtained by Licht and Pagnamenta [3] differ from those of Ji [4] by application of a factor of  $(1 + \tau)$  to  $G_E$  as well as to  $G_M$ . Alternatively, some constituent quark model calculations apply factors of  $(1 + \tau)^{1/2}$  to both form factors. Differences between these prescriptions alter the shape of the fitted density in a smooth fashion, but do not affect the qualitative relationship between the quality and range of experimental data and the precision of the fitted density, as represented by its error band. The empirical parametrization proposed by Bosted [30]

$$G \propto (1 + a_1 Q + a_2 Q^2 + a_3 Q^3 + a_4 Q^4)^{-1} \quad (8)$$

also fits the data for large  $Q^2$  well and is consistent with pQCD, but its odd powers of  $Q$  are incompatible with the interpretation of the form factor as the Fourier transform of a radial density and with the moment expansion for small  $Q^2$ . Conversely, although we cannot claim our proposed relationship between form factors and densities is model independent, it does provide a physically

appealing parametrization of the form factor data and realistic error bands in both spatial and momentum representations. Therefore, even if the identification of the extracted densities with the static densities is discounted, these densities do provide a useful parametrization of the form factors nonetheless.

In summary, we have applied the Fourier-Bessel expansion and an *ansatz* for the relationship between densities in the nucleon rest frame to transition form factors in the Breit frame to extract charge and magnetization densities with realistic estimates of their uncertainties from data for Sachs form factors. Three of the four densities are determined very accurately, but more precise data at higher  $Q^2$  will be needed to achieve comparable precision for the neutron charge density. Several new experiments using recoil or target polarization will soon provide more precise  $G_{En}$  data that should greatly improve the precision of the neutron charge density.

## ACKNOWLEDGMENTS

We thank O. Gayou for providing a table of  $G_{Ep}$  data and X. Ji and C. Perdrisat for useful discussions. The support of the U.S. National Science Foundation under grant PHY-9971819 is gratefully acknowledged.

- 
- [1] M. K. Jones *et al.*, Phys. Rev. Lett. **84**, 1398 (2000).
  - [2] O. Gayou *et al.*, nucl-ex/0111010, submitted to Phys. Rev. Lett. (unpublished).
  - [3] A. L. Licht and A. Pagnamenta, Phys. Rev. **D 2**, 1156 (1970).
  - [4] X. Ji, Phys. Lett. **B254**, 456 (1991).
  - [5] B. Dreher, J. Friedrich, K. Merle, H. Rothhaas, and G. Lührs, Nucl. Phys. **A235**, 219 (1974).
  - [6] J. L. Friar and J. W. Negele, Nucl. Phys. **A212**, 93 (1973).
  - [7] J. J. Kelly, Phys. Rev. **C 37**, 520 (1988).
  - [8] J. J. Kelly *et al.*, Phys. Rev. **C 44**, 1963 (1991).
  - [9] G. Höhler, E. Pietarinen, I. Sabba-Stefanescu, F. Borkowski, G. G. Simon, V. H. Walther, and R. D. Wendling, Nucl. Phys. **B114**, 505 (1976).
  - [10] E. J. Brash, A. Kozlov, S. Li, and G. Huber, hep-ex/0111038, submitted to Phys. Rev. C (unpublished).
  - [11] L. E. Price, J. R. Dunning, M. Goitein, K. Hanson, T. Kirk, and R. Wilson, Phys. Rev. **D 4**, 45 (1971).
  - [12] G. G. Simon, C. Schmitt, F. Borkowski, and V. H. Walther, Nucl. Phys. **A333**, 381 (1980).
  - [13] T. Eden *et al.*, Phys. Rev. **C 50**, R1749 (1994).
  - [14] I. Passchier *et al.*, Phys. Rev. Lett. **82**, 4988 (1999).
  - [15] J. Becker *et al.*, Eur. Phys. J. A **6**, 329 (1999).
  - [16] D. Rohe *et al.*, Phys. Rev. Lett. **83**, 4257 (1999).
  - [17] C. Herberg *et al.*, Eur. Phys. J. A **5**, 131 (1999).

- [18] H. Zhu *et al.*, Phys. Rev. Lett. **87**, 081801 (2001).
- [19] R. Schiavilla and I. Sick, Phys. Rev. **C 64**, 041002(R) (2001).
- [20] S. Kopecky, J. A. Harvey, N. W. Hill, M. Krenn, M. Pernicka, P. Riehs, and S. Steiner, Phys. Rev. **C 56**, 2220 (1997).
- [21] W. Xu *et al.*, Phys. Rev. Lett. **85**, 2900 (2000).
- [22] S. Rock, R. G. Arnold, P. Bosted, B. T. Chertok, B. A. Mecking, I. Schmidt, Z. M. Szalata, R. C. York, and R. Zdarko, Phys. Rev. Lett. **49**, 1139 (1982).
- [23] A. Lung *et al.*, Phys. Rev. Lett. **70**, 718 (1993).
- [24] P. Markowitz *et al.*, Phys. Rev. **C 48**, R5 (1993).
- [25] H. Anklin *et al.*, Phys. Lett. **B336**, 313 (1994).
- [26] E. E. W. Bruins *et al.* (unpublished).
- [27] H. Anklin *et al.*, Phys. Lett. **B428**, 248 (1998).
- [28] G. Kubon *et al.*, nucl-ex/0107016 (unpublished).
- [29] S. Galster, H. Klein, J. Moritz, K. Schmidt, D. Wegener, and J. Bleckwenn, Nucl. Phys. **B32**, 221 (1971).
- [30] P. E. Bosted, Phys. Rev. **C 51**, 409 (1995).

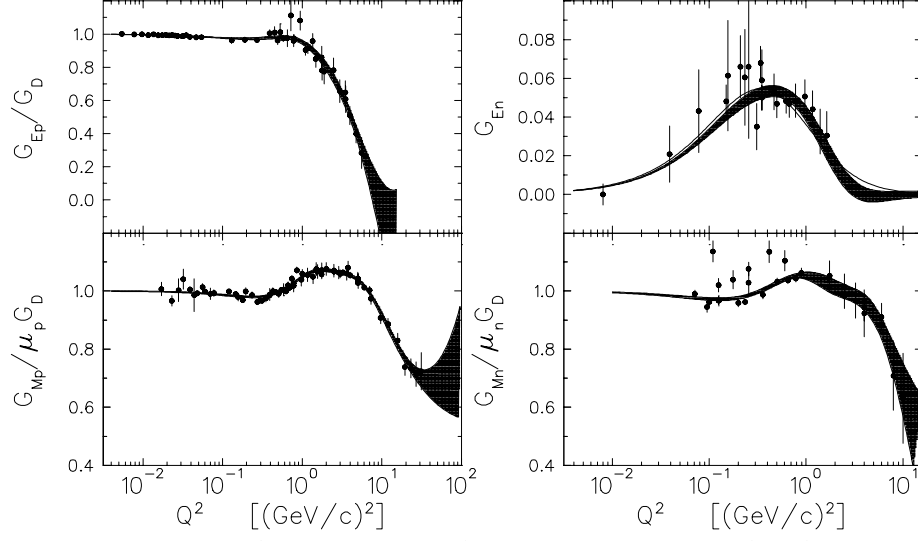


FIG. 1. The bands show Fourier-Bessel fits to selected data for nucleon electromagnetic form factors. For  $G_{En}$  the solid line shows the Galster model.

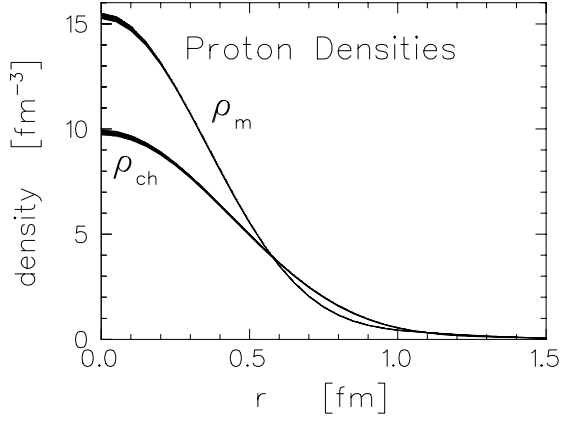


FIG. 2. Comparison between fitted charge ( $\rho_{ch}$ ) and magnetization ( $\rho_m$ ) densities for the proton. The error bands are tight and difficult to discern. Both densities are normalized to  $\int dr r^2 \rho(r) = 1$ .

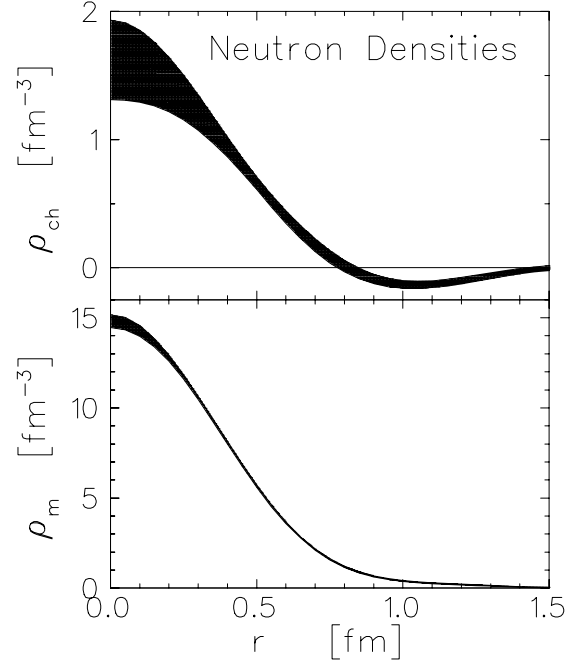


FIG. 3. Charge ( $\rho_{ch}$ ) and magnetization ( $\rho_m$ ) densities for the neutron.